Transcription of rRNA in early mouse embryos promotes chromatin reorganization and expression of major satellite repeats

Martine Chebrout[1,2,#], Maïmouna Coura Koné [1,2,3,#], Habib U. Jan[1,2,4], Marie Cournut[1,2], Martine Letheule[1,2], Renaud Fleurot[1,2,5], Tiphaine Aguirre-Lavin[1,2,6], Nathalie Peynot[1,2,7], Alice Jouneau [1,2], Nathalie Beaujean [1, 2,8] and Amélie Bonnet-Garnier [1,2*]

1) Université Paris-Saclay, UVSQ, INRAE, BREED, 78350, Jouy-en-Josas, France

2) Ecole Nationale Vétérinaire d'Alfort, BREED, 94700, Maisons-Alfort, France

3) Current address: Laboratoire Biologie et Santé, Equipe Endocrinologie et Biologie de la Reproduction animale Université Félix Houphouët - Boigny / BP V34, Abidjan 01 mounakon5@gmail.com

4) Current address: Molecular Biology, Department of Pathology, Medical Teaching Institution, Lady Reading Hospital (LRH-MTI) Peshawar Pakistan. https://orcid.org/0000-0001-9085-7398, habib.jan@lrh.edu.pk,

5) Current address: CNRS, IFCE, INRAE, Université de Tours, PRC, 37380, Nouzilly, France

6) Current address: INRAE, PAO, 37380,Nouzilly, France

7) Current address: Université Paris Saclay, INRAE, AgroParisTech, GABI, 78350 Jouy-en-Josas, France

8) Current address: Univ Lyon, Université Claude Bernard Lyon 1, Inserm, INRA, Stem Cell and Brain Research Institute U1208, USC1361, 69500 Bron, France

# The two authors contributed equally to the work.

***Corresponding author**: Amélie Bonnet-Garnier

Tel.: +33 1 34 65 23 79;

Fax: +33 1 34 65 29 09;

email: amelie.bonnet-garnier@inrae.fr

Key words: mouse, embryos, 3D-FISH, ribosomal DNA, rDNA transcription inhibition, repeated sequences.

Abstract

During the first cell cycles of the early development, the chromatin of the embryo is highly reprogrammed alongside that embryonic genome starts its own transcription. The spatial organization of the genome is a major process that contributes to regulating gene transcription in time and space, however, it is poorly studied in the context of early embryos. To study the cause and effect link between transcription and spatial organization in embryos, we focused on the ribosomal genes, that are first silent and begin to transcribe during the 2-cell stage in the mouse. We demonstrated that ribosomal sequences and early unprocessed rRNAs are spatially organized in a very peculiar manner from the 2-cell to the 16-cell. Using drugs interfering with ribosomal DNA transcription, we show that this organization, totally different from somatic cells, depends on an active transcription of ribosomal genes and induces a unique chromatin environment that favors transcription of major satellite sequences after the 4-cell stage.

Abbreviations

5'ETS: 5' externally transcribed spacer

ActD: actinomycin D

EGA: Embryonic Genome Activation

hphCG: hours post-injection of human Chorionic Gonadotrophin

H3K9ac: Histone 3 acetylated in lysine 9

H3K4me3: Histone 3 tri-methylated in lysine 4

ITS1: internal transcribed spacer 1

ITS2: internal transcribed spacer 2

Major sat: mouse major satellite sequences

NPB: Nucleolar Precursor Body

Nopp140: Nucleolar phosphoprotein of 140 kD

mPN: maternal pronucleus

pPN: paternal pronucleus

PVP: Polyvinylpyrrolidone

RT-qPCR: Real-Time quantitative PCR

RNA polymerase I: RNA pol I

rDNA: ribosomal DNA genes/sequences

rRNA: ribosomal RNA

UBF: Upstream Binding Factor

Introduction

In eukaryotes, the spatial organization of the genome within the interphasic nuclei is not random. DNA fluorescent in situ hybridization (DNA-FISH) experiments have demonstrated that chromosomes occupy a specific nuclear position called territories (Cremer

and Cremer, 2001) and that transcriptional activity influences chromosomes and genes radial positioning in the nucleus ((Therizols et al., 2014), reviewed in (Meaburn, 2016). The three-dimension (3D) organization of chromatin acts as a key component of the cell identity and can be correlated with highly differentiated cell types (Solovei et al., 2009). However, the relationships between genome organization and gene transcription are still a matter of debate, albeit after extensive studies reviewed in (van Steensel and Furlong, 2019). For a decade, chromosome conformation capture techniques (3C, 4C and Hi-C) offer the possibility to study whole-genome organization, long-distance interaction, and loops between genomic regions or loci (reviewed in (Bonev and Cavalli, 2016; Yu and Ren, 2017). But depending on the biological model, DNA-FISH and microscopy are still relevant and at least complementary to these approaches (Szabo et al., 2020) allowing single-cell analysis in intact nuclei (Gelali et al., 2019) and localization of repeated sequences such as pericentromeric and centromeric regions and ribosomal DNA (rDNA) genes (Maiser et al., 2020; Mayer et al., 2005). In mice, rDNA are located at the vinicity of major satellites sequences and depending on the mouse strand, three to four chromosome pairs (Henderson et al., 1974) are bearing nucleolus organisation region (NOR).

As for mammalian embryos, 3D-FISH approaches has been extensively used to demonstrate that pericentromeric regions (comprising minor and major satellite sequences, (Guenatri et al., 2004)) used undergo large-scale reorganization during the early embryonic development period (reviewed in (Jansz and Torres-Padilla, 2019). We and others have shown that dramatic changes occur throughout the two first cell cycles of mouse preimplantation development concomitantly with the onset of embryonic transcription (also called embryonic genome activation (EGA)) (Aguirre-Lavin et al., 2012; Bonnet-Garnier et al., 2018; Probst et al., 2007). This spatial reorganization of heterochromatin was shown to be required for further development (Casanova et al., 2013; Probst et al., 2010), highlighting its importance.

Remarkably, in 1-cell and early 2-cell mouse embryos, major (and minor) satellite sequences surround dense, spherical structures called nucleolar precursor bodies (NPBs -(Fléchon and Kopecny, 1998)). While the NPBs were first described as a seed for embryonic nucleolus to settle (Zatsepina et al., 2003), it is now believed that they serve rather as a structural platform anchoring heterochromatin and allowing its remodeling (Fulka and Langerova, 2019). At the time of EGA, satellite sequences indeed progressively disconnect from these NPBs while forming round shape clusters as found in somatic cells and called chromocenters (Aguirre-Lavin et al., 2012). Recently, (Hamdane et al., 2016) have shown that embryos lacking the nucleolar protein UBF also lack NPBs and display an abnormal distribution of heterochromatin. However, the precise relationship between these sequences and the NPBs remains unclear.

The inner organization of NPBs has been thoroughly investigated (Baran et al., 1995; Baran et al., 2001; Koné et al., 2016) by immunofluorescent staining of nucleolar proteins such as Upstream Binding Transcription Factor (UBTF), fibrillarin, B23/Nucleophosmin 1 (NPM1), and Nopp140/NOLC1 (Nucleolar and Coiled-body phosphoprotein 1) showing dynamic redistribution of the different nucleolar compartments (mainly the dense fibrillar component, (DFC) and the fibrillar center, (FC)) between the 2-cell and blastocyst stages (time of implantation). The NPBs also structurally support the ribosomal genes (rDNA) (Romanova, 2006). Remarkably, reinitiating of ribosomal transcription (rRNA synthesis) has been shown - by BrUTP incorporation (Zatsepina et al., 2003) - to occur in NPBs at the end of the 2-cell stage, when pericentromeric repeats undergo massive reorganization. It could be that the chromatin state of both rDNA and pericentromeric sequences influence each other as described in Embryonic stem cells (Guetg et al., 2010; Savić et al., 2014). Little is known regarding the spatial organization and expression of rDNA genes in the nuclei of mouse embryos.

In the somatic nuclei, the ribosomal genes are transcribed in the nucleolus by the RNA polymerase I (RNA pol I) in a long precursor transcript called 47S pre-rRNA, that will be cleaved by several endonucleases and exonucleases (Henras et al., 2008; Henras et al., 2015) to separate the internal transcribed spacers 1 (ITS1) and 2 (ITS2) and the 5′ and 3′ external transcribed spacers (5′-ETS and 3′-ETS) from the mature ribosomal RNAs (rRNAs): 18S, 5.8S, and 28S (Henras et al., 2015). These rRNAs are associated with ribosomal proteins in pre-ribosomes particles, processed/matured by several proteins, and exported in the cytoplasm to form the small and large ribosome subunits (Mullineux and Lafontaine, 2012). Two proteins: the UBF and the Selective Factor 1 (SL1) are required to load the Pol I complex and initiate transcription of the rDNA (Moss et al., 2019). Experimental disruption of the rDNA transcription can be done using either actinomycin D that intercalates into DNA at the actively transcribed rDNA sites and inhibits pre-rRNA chain elongation (Schöfer et al., 1996) or CX-5461 that inhibits transcription of rDNA genes by selectively targeting the SL1 transcription factor (Drygin et al., 2011). Studies have shown that these inhibitors can affect nucleolar structure organization, reviewed in (Grummt, 2013; Mangan et al., 2017; Potapova and Gerton, 2019).

With the use of these specific inhibitors, we will address the organization of rDNA in time and space with regard to major satellite sequences during early embryonic development by 3D-FISH. We will also analyze the expression of the various rRNA transcripts to decipher the causal relationship between the spatial organization and the expression changes of these sequences.

Results

Ribosomal genes (rDNA) 3D organization is linked to their transcription status during preimplantation development

To determine the spatial distribution of rDNA repeats concomitantly with major satellite sequences in mouse early embryo nuclei, 3D-DNA-FISH was performed using probes specific to mouse rDNA repeats (Akhmanova et al., 2000; van de Nobelen et al., 2010) and major satellite sequences (Aguirre-Lavin et al., 2012), respectively. Preservation of the 3D structure of the whole embryos with a dedicated protocol avoiding drying the embryos (see M&M section for more details) allowed us to do in-depth localization of spatial position of these sequences in the nucleus from the 1-cell to the blastocyst stage (Fig. 1A and 1C, Fig. S1A and S1B).

As expected during the 1-cell stage, major satellite sequences progressively formed a ring that surrounded NPBs (lacking DAPI staining, Fig. S1A, (Aguirre-Lavin et al., 2012). rDNA signals correspond to large foci (Fig. 1A and Fig. S1A) and are always associated with major satellite sequences irrespective of the origin of the pronucleus (mPN or pPN). At the 2-cell stage, rDNA FISH signals have a small spot shape close to large signals of major satellite sequences and can be divided into two categories: (i) some of them are not associated with NPBs (green arrows in Fig. 1A) and (ii) some of them are embedded within the ring of major satellite sequences surrounding the NPBs (black and white arrows in Fig. 1A and S1A). Interestingly, at the late 1-cell and early 2-cell (2-cell E) stages, these rDNA signals are localized at the outer edge of the NPBs (Fig. 1A) as demonstrated by plot profiles of fluorescence intensities for DAPI, major sequences, and rDNA signals across NPBs (mPN, pPN and 2 -cell E in Fig. 1B). At the end of the 2-cell stage (2-cell L) concomitantly with the embryonic genome activation (Zatsepina et al., 2003), rDNA FISH signals change in shape and localization: forming pearl necklace structures (black and white arrowhead in Fig. 1A)

juxtaposed to major satellites and extending inside the NPBs (green pick inside NPB2, plot profile at 2-cell L in Fig. 1B). The number of rDNA signals was counted in each nucleus and whatever the stage, the mean number of rDNA spots (Fig S1B) was always higher than the number of chromosome-pairs bearing NORs (7) described previously in F1 C57Bl6/JxCBA mice (Bonnet-Garnier et al., 2013; Romanova, 2006). Moreover, at early 2-cell (10 +/- 3), this mean number of spots was significantly lower than at the other stages (mPN: 12+/-4; pPN 14+/-4 and late 2-cell 13 +/- 4, Fig S1B). As the rDNA are condensed during mitosis, the sequences at the beginning of the cell cycle are likely to be more clustered than at the end (Junera et al., 1995).

From the early 4-cell to the late 8-cell stage, rDNA signals that were mostly located at the surface of NPBs, lose the pearl necklace shape to form a dispersed cloud of smaller dots, being less and less associated with major satellite sequences (Fig. 1C) and more and more inside the NPBs (as shown by plot profiles drawn across NPBs, Fig. 1D). Finally, the 3D rDNA organization changed one last time, between the 16-cell and the Morula stage: the FISH signals filled the NPBs (16-cell E, 75hphCG in Fig. S1C) and acquired a nucleolus-like structure (Morula) like in differentiated cells (Junera et al., 1995), with no differences between inner cell mass (ICM) and trophectoderm cells (TE) at the Blastocyst stage (Fig. S1C).

Quantification of the number of NPBs per stage revealed that it decreased from the late 2-cell to the 16-cell stage (black line in Fig. S1D) and that the remaining NPBs at the 16-cell stage are mostly those associated with the rDNA signal (dark blue bars in Fig. S1D). We then analyzed how rDNA organization evolved and defined four types of NPBs (Fig. 2A, upper panel): T1 corresponding to NPBs with a small number of round-shape rDNA spots; T2 corresponding to NPBs with larger spots distributed like a pearl necklace, T3 corresponding to NPBs surrounded by a thin cloud of rDNA signals and T4 corresponding to NBPS with a

larger cloud of rDNA signals. Analysis of 350 nuclei from 4-cell to 16-cell stages embryos (Fig. 2A lower panel) showed that T1 and T2 NPBs were predominant at the 4-cell stage and decreased significantly up to the late 8-cell stage (p-value < 0.005). On the other hand, T3 NPBs were mostly observed in late 4-cell and early 8-cell stages and T4 NPBs number increased significantly from 8-cell to 16-cell stage (p-value < 0.005, Mann-Whitney U test).

To complete our analysis of rDNA 3D-organization, Imaris software (version 9.6, Oxford Instruments) was used to measure the volume of rDNA FISH signals in whole embryos from the 2-cell to 16-cell stage (Fig. S1F) and the corresponding nuclear volume (stained with DAPI, Fig. S1E). To correct for the potential variation of the nuclear volumes (as show n Fig. S1E), the total rDNA volume in a nucleus was divided by the volume of this nucleus (Fig. 2B). While we did not observe variations at the 2-cell stage, earlier stages have always significantly lower normalized mean volumes than later ones at 4 and 8-cell stages (Fig 2B, S2F) potentially linked with the cell cycle since the chromatin is condensed into chromosomes during mitosis. These variations of volume between stages were confirmed by the measure of the sum of the fluorescence intensity that showed the same distribution (Fig S1G). The late 4-cell, and late 8-cell stages displayed larger rDNA volumes than earlier stages, suggesting an important decondensation of the rDNA sequences as visualized on DNA-FISH images (Fig. 1C, lower panel and Fig. 2B). Remarkably, such decondensation was confirmed by calculating the mean sphericity of rDNA spots (in a given nucleus) at each stage (Fig. 2C). Indeed, 4-cell and 8-cell stage embryos had significantly lower sphericity mean values (from 0.77to 0.82, p-value <0.005) when compared to those of 2-cell and 16-cell stage embryos (0.88 and 0.85), respectively. With regards to these parameters (rDNA volume and sphericity), the 16-cell stage has to be considered apart as the structure of the signal changes dramatically at this stage when compared to previous stages and because nuclei

become asynchronous (MacQueen and Johnson, 1983) implying that early vs. late stage cannot be distinguished anymore (Nagy et al., 2003) .

Altogether, our results showed that ribosomal genes sequences changed in shape and distribution twice during early development: first between the early and the late 2-cell stage, when rDNA becomes transcriptionally active, and, secondly, between the late 8-cell stage and the 16-cell stage on the commencement of cell differentiation.

rRNA transcription during early development

To investigate the link between 3D organization of rRNA genes and their transcriptional status, localization of probes specific to the classical rRNA components of the ribosomes subunits (18S and 28S) and to several pre-rRNA regions that correspond to pre-processed (5'ETS) or under-process rRNA (ITS1 and ITS2, detailed in Materials and Methods section and Table S1) were studied using RNA-FISH on 3D-preserved embryos (Fig. 3A and 3B).

No RNA-FISH signal were detected in the nucleus of 1-cell (data not shown) and early 2-cell stages (36hphCG, Fig 3B, 3C and 3D) irrespective of the probe used. At the late 2-cell stage, the 5'ETS signal (corresponding to the pre-processed transcripts) was located in DAPI-free regions inside the nuclei (arrowhead in Fig 3B, 2-cell embryo at 45hphCG) and at the periphery of bigger NPBs (arrow in Fig 3B). At the 4-cell and 8-cell stages, its localization shifted from the periphery to the inner part of the NPBs. Finally, at the 16-cell stage (75hphCG, Fig 3B), the 5'ETS signal filled the NPBs (Fig 3B - lower panel). As for the 5'ETS probe, the RNA-FISH signal of ITS1 and ITS2 tended to gain space inside the NPBs during progression through early embryonic development (Fig 3C and 3D). Moreover, ITS1 and 18S as well as ITS2 and 28S were completely intermingled at all stages (Fig 3C and 3D).

To complete RNA-FISH data with quantitative data, real-time quantitative PCR (RT-qPCR) using specific pre-rRNA primers (Table S2) were performed. The level of immature rRNA transcripts (assessed with 47S, 5'ETS and ITS1 specific primers), gradually increased from late 2-cell to early 8 cell stage and then the curve tends to a plateau (Fig 4A, upper panel). For ITS2 (allowing us to assess the amount of 'under-process' pre-rRNAs) a significant increase was observed from the late 4-cell to the 8-cell stage (Fig4A, lower panel).

Finally, to gain insight into a putative correlation between epigenetic marks and transcription of rDNA, we have determined using an immuno-RNA-FISH approach, the distribution of H3K9ac and H3K4me3 together with their co-localization with immature transcripts (5'ETS probes). These two histone post-translational modifications (PTMs) are canonically associated with actively transcribed genes (Allis and Jenuwein, 2016). From the 2-cell to the 8-cell stages, we observed that some H3K9ac bright foci (green arrows in Fig 4B) were localized close to 5'ETS RNA-FISH signals (white arrows in Fig 4B). Notably, H3K9ac foci were found at the periphery of 5'ETS signal at 2-cell and 4-cell stages and then dispersed in the 5'ETS cloud inside the NPBs at the 8-cell stage but did not co-localize with the totality of the immature transcripts (Fig 4B). The same results were found for H3K4me3 (green arrows in Fig S2).

Hence, our data suggest that the first part of the early development (from the late-2-cell to the 4-cell stage) is more dedicated to the initiation of rDNA transcription as revealed by a large number of immature transcripts followed, after the 8-cell stage, by an increase in the processing/cleavage of immature pre-rRNAs concomitanly with a maintenance of the initiation of transcription.

Inhibition of rRNA transcription and its consequences: elongation is impaired not initiation

To investigate this putative temporal separation of initiation of transcription and processing of rRNA, we used two inhibitors of the rRNA synthesis. Embryos at the 1-cell stage were cultured with either CX-5461 (1µM) or actinomycin D (ActD, 7.5ng/µL) and fixed 24h (2-cell stage) or 48h later (4-cell stage). We confirmed that both CX-5461-treated and ActD-treated embryos arrested their development at the 4-cell stage (Koné et al., 2016). We then localized the nascent rRNA transcripts by immunoRNA-FISH with 5'ETS probe as well as two key nucleolar components, UBF and Nopp140 involved in the initiation of rRNA transcription and processing of the pre-RNA, respectively (Koné et al., 2016). In both the treated groups, 5'ETS signal (green arrows in Fig 5A), Nopp140 (red arrows in Fig 5A), and UBF (white arrows in Fig 5A) immunoRNA-FISH patterns were altered compared to the control, untreated group (Fig 5A). As described in Koné et al (2016), in the control group of UBF and 5'ETS, signals were superposed and surrounded by Nopp140 signal and, in CX-5461-treated embryos, Nopp140 and UBF formed nucleolar caps (reviewed in (van Sluis and McStay, 2017), with 5'ETS signals still localized around NPBs. On the contrary, after 48h of treatment, ActD-treated embryos showed a higher disruption than CX-5461-treated embryos with complete segregation between the UBF-5'ETS and Nopp140 signals, suggesting that nascent transcripts were not processed anymore.

To test this hypothesis, the level of immature pre-rRNAs (using primers for 47S-pre rRNA and the 5'ETS regions) and in-processed pre-rRNAs (using primers specific to the ITS1 and the ITS2 regions) were assessed by RT-qPCR (Fig 5B and Fig 5C). There was no significant difference between control and treated embryos at the 2-cell stage. In the CX-5461 condition, the quantity of 47S, 5'ETS, and ITS1 pre-rRNAs were significantly increased (1.8 fold change) between control and the treated 4-cell embryos (Fig 5B, p value< 0.01) although

we observed a slight decrease in the RNA-FISH signal compared to control (5'ETS FISH signals in Fig 5A, ITS1 and ITS2 FISH signals in Fig 5D). A putative explanation is that CX-5461-treated embryos compensate a lower number of rDNA loci engaged in transcription by a higher rate of transcription on rDNA promoters that were able to recruit of SL1 and UBF and initiate transcription. On the contrary, we observed a significant (p-value <0.005) decrease of 5'ETS, ITS1, and ITS2 pre-rRNAs in ActD-treated embryos by RT-qPCR quantification (Fig 5C) and a modified pattern by RNA-FISH (Fig 5A and 5E). In agreement with the hypothesis that actinomycin D inhibits RNA Pol I elongation, ITS1 and ITS2 displayed a stronger reduction of RNA-FISH signals (Fig 5E) than 5'ETS (Fig 5A, left panel). CX-5461 had not a specific effect on rRNA processing compared to actinomycin D (in congruence with (Mars et al., 2020)).

Altogether, these results demonstrate that rRNA synthesis inhibition with actinomycin D treatment during early embryonic development induces transcriptional arrest at the 4-cell stage and a massive reorganization of nucleolar proteins due to an incomplete transcription and processing of the long 47S pre-rRNA.

rRNA synthesis inhibition induces changes in the 3D organization of rDNA

To assess the consequences of rRNA synthesis inhibition on rDNA organization and the nearby major satellite sequences, DNA-FISH approach was used. To compare the organization of rDNA and major satellite sequences between control (Fig. 1A et 1C) and treated embryos, the shape of both DNA signals was visualized and analyzed using 3D reconstruction at the 2-cell and 4-cell stages (Fig.6A and 6B) respectively. At the 2-cell stage, the rDNA signals were compacted and juxtaposed to major satellite signals both in control (Fig 1A) and treated embryos (green and black arrows in Fig 6A) but their position with regards to NPBs was different between control (inside NPBs, Ctrl in Fig 1B) and treated

(outside NPBs, CX-5461 and ActD in Fig 6C) embryos, as shown in plot profiles. At the 4-cell stage, the rDNA signal spatial distribution was more compact (clusters seem bigger and in lower number) in treated than in control embryos (green arrows in the upper panel, Fig 6B), and in ActD-treated embryos, it formed clusters as in 2-cell stage embryos. Plot profiles drawn across the nuclei show that rDNA signal seemed weaker in treated embryos. Moreover in the CX-5461, rDNA sequences were still inside NPBs as in the control condition, but not in the ActD condition where they were outside NPBs, juxtaposed to major satellite sequences (Fig 6D).

To assess and quantify the differences in terms of intensity, compaction and shape between the control and the treated embryos, rDNA FISH signals were segmented using Imaris software (as previously in Fig 2B and 2C) to measure the sum of intensity, the volume, and the sphericity of the rDNA signal at 2-cell and 4-cell stages (Fig 7A, 7B and 7C). In the control condition, the sum of intensity and the mean volume of the rDNA signal increased from the 2-cell to 4-cell stage, and its shape (measured by the sphericity) became less round meaning that rDNA sequences decondensed concomitantly with being actively transcribed (see also Fig 2A, 2C and S1G). At the 2-cell stage, the shape of the rDNA signal was significantly different between the control and the treated embryos (left panel in Fig 7C, p-value <0.005) suggesting that ribosomal sequences were less round in the treated embryos and putatively less compact. At the 4-cell stage, the DNA-FISH signal was less intense (Fig 7A) and the mean volume of rDNA signal was significantly (p-value <0.005) different between the control and the treated embryos (Fig 7B, 5.31 +/- 1.63 in Ctrl vs 0.85+/-0.48 and 0.93+/- 0.27 in CX-5461 and ActD treated embryos, respectively). Moreover, the mean number of segmented objects significantly (p-value <0.005) decreased between the control and the treated embryos (Fig S3A) meaning that rDNA sequences stay tightly compact and clustered when their transcription is inhibited.

Disruption of 3D organization of rDNA with rRNA synthesis inhibition has consequences on the transcription of pericentromeric sequences

By paying attention to the major satellite DNA-FISH signals (shape and volume) assisted us in pinpointing that their distribution is modified by the drug treatment. Indeed, after 48h of rRNA synthesis inhibition, major satellite DNA-FISH signals show a croissant shape- as in 2-cell embryos (red and black arrows in Fig 6B)- whereas they are normally clustered into chromocenters at the 4-cell stage in controls (Fig 1C). To confirm this further, the sum of intensity, the mean volume and the sphericity of the DNA-FISH signals of major satellite sequences were measured using Imaris in the control and the treated embryos (Fig S3B,S3C and S3D and Fig 7D, 7E and 7F). The mean volume of major satellite sequences FISH signals was significantly lower (p-value <0.005) at the 2-cell stage in treated compared to control embryos (right panel, Fig 7E). At the 4cell stage, the volume in the control decreased, while there was no change in the treated embryos (left panel, Fig 7E). Furthermore, the decreased sphericity in the treated embryos compared to the control at the 4-cell stage (right panel, Fig 7F) means that the major satellite sequences are less round and compact in the treated embryos. Similarly, the mean sphericity of the 4-cell stage in the treated embryos was not significantly different from that of the 2-cell control embryos.

Previous studies highlighted that major satellite sequences are specifically transcribed at the 2-cell stage and that is correlated with a less round DNA-FISH signal (Casanova et al., 2013; Probst et al., 2010), therefore we decided to assess major satellite transcription in the treated vs. control embryos by RNA-FISH and RT-qPCR. No difference in the major satellite RNAs was detected between the control and treated embryos at the 2-cell stage, neither by RNA-FISH nor by RT-qPCR (Fig 8A, B and C) however we detected a significant decrease of transcription in the 4-cell stage ActD-treated embryos (Fig 8B, p< 0.005). On the other hand, a housekeeping gene such as *Hprt* (Fig S3E) did not vary in ActD-treated embryos

suggesting a reciprocal influence between rDNA and major satellite transcription. As a matter of fact, after the 2-cell stage burst of transcription (Probst et al., 2010), the remaining major satellite RNA-FISH spots were always visualized inside the cloud of 5'ETS FISH signal (green arrows in Fig 8D), at the 4-cell, 8-cell, and 16-cell stages (red arrow in Fig 8D) suggesting that rDNA transcription might induce a chromatin environment that favors transcription of major satellite sequences.

Discussion

Spatial organization of rDNA during early development

In this study, we have demonstrated that ribosomal repeat sequences are first clustered at the surface of NPBs, flanked by ring-shaped major satellite sequences (1-cell and early 2-cell) before expanding in the inner space of the NPBs, until complete filling. Hence, rDNAs gradually separate spatially from their neighboring major satellite sequences. The cloudy organization of the active ribosomal sequences we observed fits with the localization of UBF as previously described (Fulka and Langerova, 2014; Hamdane et al., 2016; Koné et al., 2016) and is specific to the early embryonic period. This unique nucleolus organization is very different from the somatic ones (Maiser et al., 2020; Yao et al., 2019) that can only be found at the morula and blastocyst stages (Lavrentyeva et al., 2015). Interestingly, this second switch in the nucleolus conformation is associated with a second burst of embryonic gene transcription at the morula-to-blastocyst transition highlighted in transcriptomic data (Hamatani et al., 2004; Hamatani et al., 2006; Wang et al., 2004).

In parallel to these drastic changes in the spatial organization of the sequences, we show that rRNA synthesis begins at the mid-2-cell stage, first in the small spherical structures outside the NPBs. Therefore, at very early stages (1-cell and 2-cell stages), NPBs can not be considered as a reservoir for pre-rRNAs waiting to be cleaved, confirming previous studies

(Lavrentyeva et al., 2015; Shishova et al., 2015a; Shishova et al., 2015b). Interestingly, immuno-RNA-FISH revealed that bright spots of H3K9ac and H3K4me3 are located at the vicinity of 5'ETS signal at the 2-cell stage and then inside the 5'ETS cloud at later stages. These results are in agreement with ChIP data obtained on mouse embryonic fibroblast or 3T3 cells (Herdman et al., 2017; Zentner et al., 2014) describing an enrichment of these two epigenetic marks on the spacer promoter (UCE core) at the actively transcribed rDNA repeat (Grummt and Längst, 2013; Moss et al., 2019).

Inhibition of rRNA transcription and its impact on rRNA processing

In the early embryonic context, we observed that CX-5461 disrupts the classical tripartite (i.e. FC, DFC, and Granular component (GC) (Boisvert et al., 2007; Pederson, 2011)) nucleolus organization (this study & Koné et al 2016). Several recent studies (Bruno et al., 2020; Mars et al., 2020; Sanij et al., 2020) discussed the specific targets of CX-5461 (SL1 or Topoisomerase II or RRN3) and its mode of action (G-quadruplex stabilization, DNA damage, impairing of DNA replication fork). In agreement with (Mars et al., 2020), our study demonstrates that CX-5461 has less impact on the transcription and the elongation process than actinomycin D. In the treated embryos, actinomycin D treatment inhibits rRNA synthesis but induces a complete stop of the long pre-rRNA production (labeled with ITS1 and/or ITS2) which in turn induces both dissociation of transcription initiation (labeled by 5'ETS and UBF) and processing of rRNA (labeled with Nopp140). It is worth mentioning that the treated embryos arrested their development at the 4-cell stage most likely because maternally inherited ribosomes are not renewed as demonstrated in the embryos invalidate for UBF (Hamdane et al., 2014; Hamdane et al., 2016).

The link between major satellite and rDNA sequences transcription

Localization of major satellite sequences around the NPBs is mandatory at the 1-cell stage as demonstrated by enucleolation experiments (Fulka and Langerova, 2014; Kyogoku et al., 2014; Ogushi and Saitou, 2010; Ogushi et al., 2008) and at the early 2-cell stages (Jachowicz et al., 2013); even if in-depth knowledge of the mechanisms involved are still unknown. In this study, we show that inhibition of rDNA transcription induces major satellite sequences to change from a chromocenter-like shape to a ring-like shape. Surprisingly, actinomycin D treatment induces a decrease of major satellite transcription while other RNA polymerase II-dependent genes are not affected. These results enforce the hypothesis of a physical link between these two events. Growing pieces of evidence indeed propose that NPBs, rather than acting as a precursor of nucleoli, act as a platform or a Velcro for major satellite sequences (Fulka and Aoki, 2016; Padeken and Heun, 2014) thanks to nucleoplasmin 2 (NPM2, (Burns et al., 2003; Inoue and Aoki, 2010; Kyogoku et al., 2014)). In fact injection of sole NPM2 mRNA rescue developmental failure of enucleolated oocytes (Ogushi et al., 2017).

We also showed that rDNA spatial organization is disrupted when their transcription is inhibited and rDNA aggregate, exhibiting a round shape comparable to earlier inactive stages. Similarly, major satellite sequences exhibit a spatial organization that looks like an early 2-cell stage. This loss of chromatin organization in rRNA transcription inhibited embryos can partially explain the decrease of major satellite sequence transcription. After the 2-cell stage, major satellite transcription is severely repressed and only one or two spots of major satellite RNA can be detected per nucleus by RNA-FISH (Probst et al., 2010). Remarkably, these spots were often found inside the 5'ETS cloud (this study), suggesting transcription of major satellite sequences after the 2-cell stage may require a suitable environment that favors transcription. A putative explanation -among others- is that transcription of major satellite

sequences, in 4-cell and 8-cell embryos, need the rDNA peculiar chromatin state (Moss et al., 2019; Potapova and Gerton, 2019): nucleosome-free chromatin with UBF that promotes loops formation (Stefanovsky et al., 2001).

Material and Methods

Ethics

Animal care and handling were carried out according to the national rules on ethics and animal welfare in the Animal facility (IERP, INRAE, Infectiology of fishes and rodent facility, doi: 10.15454/1.5572427140471238E12, Jouy-en-Josas, C78-720). This work was approved by the French Ministry of Higher Education, Research and Innovation (n°15-55) and the local ethical committee (INRAE Jouy-en-Josas Center). Departmental veterinary regulatory services have delivered habilitation to work with laboratory animals to ABG (n°78–184) who supervised the work.

Collection of mouse embryos and culture

Embryos were collected upon superovulation and mating of C57/CBAF1 mice as previously described (Koné et al., 2016). Zygotes were obtained by dissecting the ampulla of the oviduct 24 hours post-injection of human chorionic gonadotropin (hCG) and treated briefly with 1mg/ml of hyaluronidase (Sigma) in M2 medium (Sigma) to remove follicular cells. Then, 1-cell (24h phCG) embryos were cultured *in vitro* in M16 medium (Sigma) at 37°C in a humidified atmosphere of 5% CO_2 until they reached the adequate stages (according to our previous publication, (Aguirre-Lavin et al., 2012; Koné et al., 2016) to be processed: early 2-cell (36h phCG - 2CE), late 2-cell (48h phCG - 2CL), early 4-cell (54h phCG - 4CE), late 4-cell (58h phCG - 4CL), early 8-cell (60h phCG - 8CE), late 8-cell (72h phCG - 8CL), 16-cell (75h phCG), Morula (96h phCG) and Blastocyst (110h phCG). Early and late stages are

defined as before the S-phase so in G1 (early) or in G2 (late) after the S-phase of the cell cycle. The pick-up of the embryos at a specific hour post-hCG injection is based on the knowledge of the timing of cleavages and the length cell cycle during the mouse early development (West, 1995).

CX-5461 and actinomycin D treatment

Two different drugs inhibiting rRNA synthesis were used in this study. First, CX-5461 that was first described (Drygin et al., 2011) as impairing the assembly of the RNA Polymerase I pre-initiation complex (PIC) by disrupting the recruitment of SL1 (Selective factor 1) and UBF (Upstream biding factor) to the rDNA promoter but can also induce DNA damage by stabilization of G-quadruplex (Xu et al 2017) and targets Topoisomerase II (Bruno et al., 2020) and second actinomycin D that binds GC-rich loci, intercalates into the DNA and thereby inhibits elongation of RNA polymerases activity, although with a higher affinity for RNA Pol I (Bensaude, 2011; Perry and Kelley, 1970). These two drugs induce segregation of the nucleolus components dedicated either to transcription (fibrillar and dense fibrillar components -FC and DFC) or to rRNA processing (granular component, GC). These components can be visualized by fluorescent immuno-detection of the proteins involved in these processes (UBF and Nopp140 respectively, as described in (Koné et al., 2016)).

Embryos collected at the 1-cell stage (24hphCG) were cultured in M16 medium containing either 1µM of CX-5461 (Adooq) or 7.5ng/µL of actinomycin D (Sigma) as described respectively in (Bellier, 1997; Koné et al., 2016). Every 24h, the embryos were transferred into new droplets of medium containing the drugs. The treated embryos were fixed at two-time points: 24h and 48h after exposure to the drug and then processed for immunoRNA-FISH / DNA-FISH or frozen dry in low RNA binding tubes and kept at -80°C for RT-qPCR assays.

Probes for DNA and RNA-FISH

rDNA and major satellite FISH probes were prepared as described in (Aguirre-Lavin et al., 2012) and (Bonnet-Garnier et al., 2013). Briefly, cosmid containing the entire transcribed sequences (n°13, detailed in (Akhmanova et al., 2000; van de Nobelen et al., 2010) was used for the ribosomal sequences (kind gift from N. Galjart, Department of Cell Biology, Erasmus University Medical Center, Rotterdam, The Netherlands). The amplified rDNA gene fragments were purified using nucleobond AX 100 columns for Miniprep System (Macherey-Nagel, Ref 740521.100). The rDNA sequences were then labeled with Digoxigenin-11-dUTP by nick translation according to the manufacturer's protocol (Roche, Ref 11277065910). For the detection of major satellites, a probe prepared by PCR on genomic mouse DNA with the primers 5'-CATATTCCAGGTCCTTCAGTGTGC-3' and 5'-CACTTTAGGACGTGAAAT ATGGCG-3' was labeled with Cy3 by random priming according to the kit instruction (Invitrogen Kit, Ref 18095–011).

Specific oligo-probes (designed from the complete 45S mouse ribosomal sequences - X82564.1 or adapted from (Le Bouteiller et al., 2013; Shishova and others, 2011; Shishova et al., 2015b) directly labeled with a fluorophore in 3' end (sequences are detailed in Table S1) were purchased from Eurogentec. These probes located (Fig. 2B) on different regions of the 47S pre-RNA (Kent et al., 2008) are named: 5'ETS for the probe specific to the external transcribed spacer (rapidly removed, allowing the detection of immature transcripts), ITS1: specific for the internal transcribed spacer 1 located between the 18S and the 5.8S regions and ITS2: specific for the internal transcribed spacer 2 located between the 5.8S and the 28S region. ITS1 and ITS2 enable the localization of rRNA underprocessing. Probes specific for 18S and 28S regions were also used to assess if mature or pre-rRNAs were already accumulated in NPBs before the onset of rDNA transcription. Of note, the 18S and 28S probes signal can be detected in the cytoplasm because they are components of ribosomes.

DNA-FISH

For DNA-FISH, DNA probes described above specific to either ribosomal or major satellite sequences were used together on the whole embryos. During all the manipulations, drying was avoided to preserve the 3D of nuclei. This protocol is based on (Miyanari and Torres-Padilla, 2012) with slight modifications. The embryos collected at a specific stage were transferred in a 10-well glass dish warm at 37°C. The embryos were rinsed in M2 medium, submitted briefly (less than 15s) to Tyrode's acid solution (Sigma-Aldrich), washed quickly in an M2 with 10mM phenylmethanesulfonyl fluoride (PMSF, Fluka) solution then in a 0.5% polyvinyl-pyrrolidone (PVP) in PBS with 10mM PMSF solution and finally incubated in a fixation/permeabilization solution (4% paraformaldehyde solution in PBS (PFA), 0.5% Triton X-100, 10mM PMSF, 0.5% PVP in PBS) for 15min at 37°C. The embryos were then washed twice in a PBS/PVP 0.5% solution at RT and let at +4°C (at least overnight) in a humid chamber until fixation of other stages. To remove the zona pellucida (ZP), all the embryos were incubated under a stereomicroscope to monitor the ZP vanishing in a 0.1N HCl (Prolabo) solution for 20 to 30s (depending on the stage) at RT and transferred to PBS/PVP 0.5%. The ZP removal was achieved by successive passages through a very fine glass pipette when needed. The embryos were permeabilized in a 0.5% Triton X-100 / 200µg/ml RNase solution for 30 min at 37°C and washed twice in 2X saline-sodium citrate (2XSSC) pH 6.3 for 5 min at 37°C. The embryos were then transferred for 3h at 37°C in a humidified chamber in a 20µl drop of hybridization buffer (50% formamide, SCC 2X, Denhardt 1X, 40 mM NaH2PO4, 10% dextran sulfate) containing the DNA-FISH probes mix (14µl of rDNA probe solution at 50ng/µl and 1µl of major satellite probe solution at 100 ng/µl completed to 20µl with hybridization buffer). The embryos were denatured at 85°C for 10 min on a heating plate and then let three days for hybridization at 37°C in a humid chamber. After hybridization, the embryos were rinsed twice with 2X SSC / 0.1% Triton X-100 / 0.5% PVP for 10 min at 42°C.

Embryos were then incubated in a blocking solution (4X SSC / 2% BSA) for 1h at RT and incubated with a primary antibody diluted in blocking solution (sheep anti-digoxigenin, 1/200, Roche) overnight at +4°C in a dark humidified chamber. The embryos were washed twice in 4X SSC / 2% BSA / 0.05% Tween20 before and after incubation with the secondary antibody (mouse anti-sheep Ig coupled to FITC, 1/200, 713-095-147, Jackson ImmunoResearch Laboratories Inc., USA) for 1h at RT. The embryos were washed in 2X SSC / 0.5% PVP and gently mounted to preserve the 3D structure of the nuclei between slides (Menzel Superfrost Plus, Thermo Scientific) and cover-slip with a large amount of Vectashield antifading agent (Abcys) containing 10µg/mL DAPI (Invitrogen).

RNA-FISH

For RNA-FISH, the embryos were processed almost as for DNA-FISH with three main differences: 1) the ZP was not removed by HCl treatment; 2) an RNAse inhibitor (1µL/mL of RNasin - Promega) was added to all the solutions after the fixation/permeabilization step and more importantly, the embryos were not submitted to denaturation at 85°C i.e. only the probes are heat-denaturated, not the DNA of the embryos. Briefly, after fixation/permeabilization, embryos were further permeabilized in 0.5% Triton X100 /0.5% PVP-PBS for 45min at 37°C, washed and transferred for 30min at 50°C in the pre-hybridization mix containing 50% formamide (Sigma-Aldrich); 0.5µg/µL tRNA (Sigma-Aldrich); 1X hybridization buffer (2X hybridization buffer was prepared beforehand with 20% dextran sulfate, 4X SSC; 1mM EDTA, 40mg/mL BSA, 2mg/mL PVP, 0.1% Triton X100, diluted in water). In parallel, a solution containing the fluorescent oligonucleotide probes (100ng/µl diluted in 1X hybridization buffer) was denatured 10 min at 85°C and immediately put on ice to avoid renaturation of the DNA. The embryos were then transferred in this hybridization mix and incubated overnight at 37°C. The embryos were washed twice in 2XSSC; 0.5%PVP; 0.1%

Triton X100 (diluted with pure grade water) for 10min at 37°C and mounted on slides with coverslips as described in the DNA-FISH section. The figure S4 shows a positive control of the RNA-FISH procedure (first panel) in regards with embryos incubated with RNase that correspond to the negative control (middle panel). The last panel allows the comparison between major satellite DNA-FISH signals and major satellite RNA-FISH signals (first panel).

ImmunoRNA-FISH

Immunofluorescence labeling followed by RNA-FISH was performed as described in Koné et al. (2016) with slight modifications. Briefly, the embryos were fixed as described in the RNA-FISH section before immunostaining. The embryos were then permeabilized in 0.5% Triton X100 / 0.5% PVP-PBS for 30min at 37°C and transferred in 2% BSA-PBS 1h at RT. The embryos were incubated with primary antibody overnight at 4°C, washed thrice in 0.5%PVP-PBS, and then incubated with secondary antibody for 1h and post-fixed in 2% PFA/0.5% PVP-PBS for 10 min at RT. The embryos were then further processed for RNA-FISH as described in the RNA-FISH section. All antibodies were diluted in 2% BSA-PBS. Again, RNAse inhibitor (1µL/mL of RNasin - Promega) was added to all the solutions after the fixation/permeabilization step.

Antibodies

Primary antibodies used: anti-UBF (1/100; mouse polyclonal antibody H00007343-M01; Novus Biologicals), anti-Nopp140 (1/150; rabbit polyclonal antibody, RF12 serum; a gift from U. Thomas Meier, Department of Anatomy and Structural Biology, Albert Einstein College of Medicine, New York, USA), anti-H3K9ac (1/100, rabbit polyclonal antibody, 39917) and anti-H3K4me3 (1/400, rabbit polyclonal antibody, ab8550, Abcam). Secondary

antibodies used: IgG donkey anti-mouse Cy3 (1/200, 715-025-151, Jackson ImmunoResarch) and IgG donkey anti-rabbit Cy5 (1/200, 111-175-152, Jackson ImmunoResarch).

Confocal microscopy and image analyses

Imaging was performed with a ZEISS LSM 700 confocal laser scanning microscope (MIMA2, INRAE, Microscopy and Imaging Facility for Microbes, Animals and Foods, https://doi.org/10.15454/1.5572348210007727E12) equipped with a 63X (1.4 NA) oil immersion objective. Z-stacks were acquired with a frame size of 512 × 512 or 1024 x 1024, a pixel depth of 8 bits, and a z-distance of 0.37 µm between optical sections. Wavelengths of 405, 488, 555, and 639 nm were used to excite DAPI, Alexa-488, or FITC, Cy3, and Cy5, respectively. Images constist in a stack of 40 to 80 z positions spaced of 0.37µm and are in average of 22µm of thickness.

Fluorescent profiles measurement were generated in Fiji (Schindelin et al., 2012; Schindelin et al., 2015; Schneider et al., 2012) and 3D reconstructions using AMIRA 3.1 software (Mercury Computer Systems, Berlin, Germany, (Stalling et al.)

Quantitative image analysis was performed manually using Imaris 9.6 software (Oxford Instruments) available at the MIMA2 ISC INRAE. Briefly, in 10 to 15 embryos of each stage, nuclei were first segmented using an adjusted threshold (wizard function in Imaris surfaces package). Thresholds are automatically proposed by the Imaris wizard function accordingly to the absolute intensity dynamic in a given image (Fig S5A) and allow the best separation between signal and background noise. Major satellites and rDNA signals (Fid S5B) were then segmented in a specified region of interest (ROI defined by the nucleus label) following the same process. For all detected objects, several values (sum of the intensity, volume, sphericity, numbers) were calculated by Imaris and exported for statistical analysis in Microsoft Excel file format. For each analyzed nuclei, the sum of the volume of DNA-FISH

signals was calculated to obtain the total volume of rDNA or major satellite DNA-FISH signals in a given nucleus. Then this total volume was normalized by the volume of the given nucleus using this formula: (Vol_tot_{FISH} / $Vol\_tot_{nucleus}$)x 100, to circumvent any nucleus size effect when comparing between stages.

RT-qPCR

The embryos at each stage were pooled by a batch of 10 and snap-frozen. Total RNA was prepared without purification using the SingleShot Cell Lysis kit (Biorad) that includes DNase treatment. cDNA was prepared directly from the lysates with random hexamers (300 ng) (Lifetechnologies, France) following the supplier's protocol (25°C for 5 min, 50°C for 60 min and 70°C for 15 min) in the presence of 10 fg of Luciferase RNA (Promega) using the SuperSript III reverse transcription kit (Invitrogen). Negative controls without reverse transcriptase were prepared the same way. RT-qPCR was performed on 0.2 or 0.032 embryo equivalent (as described in Salvaing et al 2016), depending on the genes, using KAPA SYBR FAST (Roche) or SYBR Green (Applied, for Major satellites) master mix on a StepOne Plus cycling machine (Applied). The difference in amplification of positive and negative samples was at least 5 Ct (5 to 9). To avoid biais due to a highly variable amount of transcript from endogenous genes (Hprt1) before the EGA, the results were finally normalized to Luciferase (as described in (Bui et al., 2009). Primers are listed in Table S2. Three to six biological replicates were used.

Statistical analyses

All the statistical analyses and tests were performed using R packages. Several R packages such as ggplot2 and lattice were used in complement to Rcmdr packages to generate graphs. The normality and homogeneity of variances were tested using the 'shapiro.test' and

'bartlett.test' R-packages, respectively. As the sample size was small (<30), non-parametrical tests were used. Two by two comparison were done using 'wilcox' packge (Mann-Whitney-Wilcoxon) and comparison of the two consecutive stages were done with 'nparcomp' package (Nonparametric Multiple Comparisons).

Supplementary material

Figs. S1–S5 show 3D organization of ribosomal sequences (rDNA) at 1-cell stage, 16-cell and morula to blastocyst stages using DNA-FISH, the mean number if rDNA cluster at 1-cell to 2-cell stages, the number of nucleolar precursor bodies (NPBs), Quantification of the sum of the intensities and the volume of nucleus and rDNA FISH signals using Imaris, Localization of H3K4me3 and immature transcripts of rRNA by immunoRNA-FISH, Quantification of mean number of rDNA-FISH objects in control and treated embryos, Quantification of major satellite sequences : the sum of the intensity, volume and sphericity from 2-cell up to 16-cell stage and relative expression of an housekeeping gene (*Hprt*) by RT-qPCR in control and treated embryos. Description of the workflow used to segment DNA and rDNA the images.

Tables S1–S2 show the list of oligoprobes used for the RNA-FISH and the list of primers used in th RT-qPCR experiments respectively.

Acknowledgements

We would like to thank Prof. Galjart Niels (Nederland), M Cohen-Tanoudji (Pasteur Institute), and Janice Britton Davidian lab (Montpellier) for their kind gifts of rDNA plasmids/cosmids and the RNA-FISH probes. We also thank Claire Boulesteix for her technical assistance and laboratory facilities and Bertrand Bed'hom for his help with Excel analysis. We thank the ISC MIMA2 (Microscopy and Imaging Facility for Microbes, Animals and Foods, doi: 10.15454/1.5572348210007727E12) and particularly Pierre Adenot for advice in acquisition of images and 3D analyses with ImageJ and Imaris. We acknowledge the staff of the INRAE Infectiology of Fishes and Rodents Facility (IERP-UE907, Jouy-en-Josas Research Center, France) in which animal experiments have been performed. IERP

Facility belongs to the National Distributed Research Infrastructure for the Control of Animal and Zoonotic Emerging Infectious Diseases through In Vivo Investigation (EMERG'IN DOI: 10.15454/1.5572352821559333E12).

This project was funded by the REVIVE Labex (Investissement d'Avenir, ANR-10-LABX-73) and supported by the PHASE Department of the French National Research Institute for Agriculture, Food and Environment (INRAE).

The authors declare no competing financial interests.

Authors contribution

M. Chebrout set up the RNA-FISH and immunoRNA-FISH experiments, performed majority of the experiments, and analyzed the data. M.C. Koné, M. Cournut and H.U Jan performed and analyzed DNA-FISH experiments. R. Fleurot and T. Aguirre-Lavin set up and performed the DNA-FISH experiments. A. Jouneau and N. Peynot performed and analyzed the RT-qPCR experiments. N. Beaujean secured funding, supervised part of the experiments and their analysis, and participated in the writing process. A. Bonnet-Garnier supervised, directed, and designed the study, analyzed, and interpreted the data, made the figures, and wrote the article. All the authors reviewed and commented on the manuscript.

Ethical approval

All applicable international, national, and/or institutional guidelines for the care and use of animals were followed. This article does not contain any studies with human participants performed by any of the authors.

References

Aguirre-Lavin, T., Adenot, P., Bonnet-Garnier, A., Lehmann, G., Fleurot, R., Boulesteix, C., Debey, P. and Beaujean, N. (2012). 3D-FISH analysis of embryonic nuclei in mouse highlights several abrupt changes of nuclear organization during preimplantation development. *BMC Dev. Biol.* **12**, 30.

Akhmanova, A., Verkerk, T., Langeveld, A., Grosveld, F. and Galjart, N. (2000). Characterisation of transcriptionally active and inactive chromatin domains in neurons. *J. Cell Sci.* **113**, 4463–4474.

Allis, C. D. and Jenuwein, T. (2016). The molecular hallmarks of epigenetic control. *Nat. Rev. Genet.*

Baran, V., Veselá, J., Rehák, P., Koppel, J. and Fléchon, J. E. (1995). Localization of fibrillarin and nucleolin in nucleoli of mouse preimplantation embryos. *Mol Reprod Dev* **40**,.

Baran, V., Brochard, V., Renard, J. P. and Flechon, J. E. (2001). Nopp 140 involvement in nucleologenesis of mouse preimplantation embryos. *Mol. Reprod. Dev.* **59**, 277–284.

Bellier, S. (1997). Nuclear translocation and carboxyl-terminal domain phosphorylation of RNA polymerase II delineate the two phases of zygotic gene activation in mammalian embryos. *EMBO J.* **16**, 6250–6262.

Bensaude, O. (2011). Inhibiting eukaryotic transcription. Which compound to choose? How to evaluate its activity?: Which compound to choose? How to evaluate its activity? *Transcription* **2**, 103–108.

Boisvert, F.-M., van Koningsbruggen, S., Navascués, J. and Lamond, A. I. (2007). The multifunctional nucleolus. *Nat. Rev. Mol. Cell Biol.* **8**, 574–585.

Bonev, B. and Cavalli, G. (2016). Organization and function of the 3D genome. *Nat. Rev. Genet.* **17**, 661–678.

Bonnet-Garnier, A., Feuerstein, P., Chebrout, M., Fleurot, R., Jan, H.-U., Debey, P. and Beaujean, N. (2013). Genome organization and epigenetic marks in mouse germinal vesicle oocytes. *Int. J. Dev. Biol.* **56**, 877–887.

Bonnet-Garnier, A., Kiêu, K., Aguirre-Lavin, T., Tar, K., Flores, P., Liu, Z., Peynot, N., Chebrout, M., Dinnyés, A., Duranthon, V., et al. (2018). Three-dimensional analysis of nuclear heterochromatin distribution during early development in the rabbit. *Chromosoma* **127**, 387–403.

Bruno, P. M., Lu, M., Dennis, K. A., Inam, H., Moore, C. J., Sheehe, J., Elledge, S. J., Hemann, M. T. and Pritchard, J. R. (2020). The primary mechanism of cytotoxicity of the chemotherapeutic agent CX-5461 is topoisomerase II poisoning. *Proc. Natl. Acad. Sci.* **117**, 4053–4060.

Bui, L. C., Evsikov, A. V., Khan, D. R., Archilla, C., Peynot, N., Hénaut, A., Le Bourhis, D., Vignon, X., Renard, J. P. and Duranthon, V. (2009). Retrotransposon expression as a defining event of genome reprograming in fertilized and cloned bovine embryos. *REPRODUCTION* **138**, 289–299.

Burns, K. H., Viveiros, M. M., Ren, Y., Wang, P., DeMayo, F. J., Frail, D. E., Eppig, J. J. and Matzuk, M. M. (2003). Roles of NPM2 in chromatin and nucleolar organization in oocytes and embryos. *Science* **300**, 633–6.

Casanova, M., Pasternak, M., El Marjou, F., Le Baccon, P., Probst, A. V. and Almouzni, G. (2013). Heterochromatin Reorganization during Early Mouse Development Requires a Single-Stranded Noncoding Transcript. *Cell Rep.* **4**, 1156–1167.

Cremer, T. and Cremer, C. (2001). Chromosome territories, nuclear architecture and gene regulation in mammalian cells. *Nat Rev Genet* **2**, 292–301.

Drygin, D., Lin, A., Bliesath, J., Ho, C. B., O'Brien, S. E., Proffitt, C., Omori, M., Haddach, M., Schwaebe, M. K., Siddiqui-Jain, A., et al. (2011). Targeting RNA Polymerase I with an Oral Small Molecule CX-5461 Inhibits Ribosomal RNA Synthesis and Solid Tumor Growth. *Cancer Res.* **71**, 1418–1430.

Fléchon, J.-E. and Kopecny, V. (1998). The nature of the 'nucleolus precursor body' in early preimplantation embryos: a review of fine-structure cytochemical, immunocytochemical and autoradiographic data related to nucleolar function. *Zygote* **6**, 183–191.

Fulka, H. and Aoki, F. (2016). Nucleolus Precursor Bodies and Ribosome Biogenesis in Early Mammalian Embryos: Old Theories and New Discoveries1. *Biol. Reprod.* **94**,.

Fulka, H. and Langerova, A. (2014). The maternal nucleolus plays a key role in centromere satellite maintenance during the oocyte to embryo transition. *Development* **141**, 1694–1704.

Fulka, H. and Langerova, A. (2019). Nucleoli in embryos: a central structural platform for embryonic chromatin remodeling? *Chromosome Res.* **27**, 129–140.

Gelali, E., Girelli, G., Matsumoto, M., Wernersson, E., Custodio, J., Mota, A., Schweitzer, M., Ferenc, K., Li, X., Mirzazadeh, R., et al. (2019). iFISH is a publically available resource enabling versatile DNA FISH to study genome architecture. *Nat. Commun.* **10**, 1636.

Grummt, I. (2013). The nucleolus—guardian of cellular homeostasis and genome integrity. *Chromosoma* **122**, 487–497.

Grummt, I. and Längst, G. (2013). Epigenetic control of RNA polymerase I transcription in mammalian cells. *Biochim. Biophys. Acta BBA-Gene Regul. Mech.* **1829**, 393–404.

Guenatri, M., Bailly, D., Maison, C. and Almouzni, G. (2004). Mouse centric and pericentric satellite repeats form distinct functional heterochromatin. *J. Cell Biol.* **166**, 493–505.

Guetg, C., Lienemann, P., Sirri, V., Grummt, I., Hernandez-Verdun, D., Hottiger, M. O., Fussenegger, M. and Santoro, R. (2010). The NoRC complex mediates the heterochromatin formation and stability of silent rRNA genes and centromeric repeats. *EMBO J* **29**,.

Hamatani, T., Carter, M. G., Sharov, A. A. and Ko, M. S. H. (2004). Dynamics of global gene expression changes during mouse preimplantation development. *Dev Cell* **6**,.

Hamatani, T., Ko, M. S., Yamada, M., Kuji, N., Mizusawa, Y., Shoji, M., Hada, T., Asada, H., Maruyama, T. and Yoshimura, Y. (2006). Global gene expression profiling of preimplantation embryos. *Hum. Cell* **19**, 98–117.

Hamdane, N., Stefanovsky, V. Y., Tremblay, M. G., Németh, A., Paquet, E., Lessard, F., Sanij, E., Hannan, R. and Moss, T. (2014). Conditional Inactivation of Upstream Binding Factor Reveals Its Epigenetic Functions and the Existence of a Somatic Nucleolar Precursor Body. *PLoS Genet.* **10**, e1004505.

Hamdane, N., Tremblay, M. G., Dillinger, S., Stefanovsky, V. Y., Németh, A. and Moss, T. (2016). Disruption of the UBF gene induces aberrant somatic nucleolar bodies and disrupts embryo nucleolar precursor bodies. *Gene*.

Henderson, A. S., Eicher, E. M., Yu, M. T. and Atwood, K. C. (1974). The chromosomal location of ribosomal DNA in the mouse. *Chromosoma* **49**, 155–160.

Henras, A. K., Soudet, J., Gérus, M., Lebaron, S., Caizergues-Ferrer, M., Mougin, A. and Henry, Y. (2008). The post-transcriptional steps of eukaryotic ribosome biogenesis. *Cell. Mol. Life Sci.* **65**, 2334–2359.

Henras, A. K., Plisson-Chastang, C., O'Donohue, M.-F., Chakraborty, A. and Gleizes, P.-E. (2015). An overview of pre-ribosomal RNA processing in eukaryotes: Pre-ribosomal RNA processing in eukaryotes. *Wiley Interdiscip. Rev. RNA* **6**, 225–242.

Herdman, C., Mars, J.-C., Stefanovsky, V. Y., Tremblay, M. G., Sabourin-Felix, M., Lindsay, H., Robinson, M. D. and Moss, T. (2017). A unique enhancer boundary complex on the mouse ribosomal RNA genes persists after loss of Rrn3 or UBF and the inactivation of RNA polymerase I transcription. *PLoS Genet.* **13**, e1006899.

Inoue, A. and Aoki, F. (2010). Role of the nucleoplasmin 2 C-terminal domain in the formation of nucleolus-like bodies in mouse oocytes. *FASEB J. Off. Publ. Fed. Am. Soc. Exp. Biol.* **24**, 485–494.

Jachowicz, J. W., Santenard, A., Bender, A., Muller, J. and Torres-Padilla, M.-E. (2013). Heterochromatin establishment at pericentromeres depends on nuclear position. *Genes Dev.* **27**, 2427–2432.

Jansz, N. and Torres-Padilla, M.-E. (2019). Genome activation and architecture in the early mammalian embryo. *Curr. Opin. Genet. Dev.* **55**, 52–58.

Junera, H. R., Masson, C., Geraud, G. and Hernandez-Verdun, D. (1995). The three-dimensional organization of ribosomal genes and the architecture of the nucleoli vary with G1, S and G2 phases. *J. Cell Sci.* **108**, 3427–3441.

Kent, T., Lapik, Y. R. and Pestov, D. G. (2008). The 5' external transcribed spacer in mouse ribosomal RNA contains two cleavage sites. *RNA* **15**, 14–20.

Koné, M. C., Fleurot, R., Chebrout, M., Debey, P., Beaujean, N. and Bonnet-Garnier, A. (2016). Three-Dimensional Distribution of UBF and Nopp140 in Relationship to Ribosomal DNA Transcription During Mouse Preimplantation Development1. *Biol. Reprod.* **94**,.

Kyogoku, H., Fulka, J., Wakayama, T. and Miyano, T. (2014). De novo formation of nucleoli in developing mouse embryos originating from enucleolated zygotes. *Development* **141**, 2255–2259.

Lavrentyeva, E., Shishova, K., Kagarlitsky, G. and Zatsepina, O. (2015). Localisation of RNAs and proteins in nucleolar precursor bodies of early mouse embryos. *Reprod. Fertil. Dev.*

Le Bouteiller, M., Souilhol, C., Beck-Cormier, S., Stedman, A., Burlen-Defranoux, O., Vandormael-Pournin, S., Bernex, F., Cumano, A. and Cohen-Tannoudji, M. (2013). Notchless-dependent ribosome synthesis is required for the maintenance of adult hematopoietic stem cells. *J. Exp. Med.* **210**, 2351–2369.

MacQueen, H. A. and Johnson, M. H. (1983). The fifth cell cycle of the mouse embryo is longer for smaller cells than for larger cells. *J. Embryol. Exp. Morphol.* **77**, 297–308.

Maiser, A., Dillinger, S., Längst, G., Schermelleh, L., Leonhardt, H. and Németh, A. (2020). Super-resolution in situ analysis of active ribosomal DNA chromatin organization in the nucleolus. *Sci. Rep.* **10**, 7462.

Mangan, H., Gailín, M. Ó. and McStay, B. (2017). Integrating the genomic architecture of human nucleolar organizer regions with the biophysical properties of nucleoli. *FEBS J.* **284**, 3977–3985.

Mars, J.-C., Tremblay, M. G., Valere, M., Sibai, D. S., Sabourin-Felix, M., Lessard, F. and Moss, T. (2020). The chemotherapeutic agent CX-5461 irreversibly blocks RNA polymerase I initiation and promoter release to cause nucleolar disruption, DNA damage and cell inviability. *NAR Cancer* **2**,.

Mayer, R., Brero, A., von Hase, J., Schroeder, T., Cremer, T. and Dietzel, S. (2005). Common themes and cell type specific variations of higher order chromatin arrangements in the mouse. *BMC Cell Biol.* **6**, 44.

Meaburn, K. J. (2016). Spatial Genome Organization and Its Emerging Role as a Potential Diagnosis Tool. *Front. Genet.* **7**,.

Miyanari, Y. and Torres-Padilla, M. E. (2012). Control of ground-state pluripotency by allelic regulation of Nanog. *Nature* **483**, 470–3.

Moss, T., Mars, J.-C., Tremblay, M. G. and Sabourin-Felix, M. (2019). The chromatin landscape of the ribosomal RNA genes in mouse and human. *Chromosome Res.* **27**, 31–40.

Mullineux, S.-T. and Lafontaine, D. L. J. (2012). Mapping the cleavage sites on mammalian pre-rRNAs: Where do we stand? *Biochimie* **94**, 1521–1532.

Nagy, A., Gertsenstein, M., Vintersten, K. and Behringer, R. (2003). *Manipulating the mouse embryo: a laboratory manual, 3rd edition*. Cold spring harbor laboratory Cold Spring Harbor, NY.

Ogushi, S. and Saitou, M. (2010). The nucleolus in the mouse oocyte is required for the early step of both female and male pronucleus organization. *J. Reprod. Dev.* **56**, 495–501.

Ogushi, S., Palmieri, C., Fulka, H., Saitou, M., Miyano, T. and Fulka, J. (2008). The Maternal Nucleolus Is Essential for Early Embryonic Development in Mammals. *Science* **319**, 613.

Ogushi, S., Yamagata, K., Obuse, C., Furuta, K., Wakayama, T., Matzuk, M. M. and Saitou, M. (2017). Reconstitution of the oocyte nucleolus in mice through a single nucleolar protein, NPM2. *J. Cell Sci.* **130**, 2416–2429.

Padeken, J. and Heun, P. (2014). Nucleolus and nuclear periphery: Velcro for heterochromatin. *Curr. Opin. Cell Biol.* **28**, 54–60.

Pederson, T. (2011). The Nucleolus. *Cold Spring Harb. Perspect. Biol.* **3**, a000638–a000638.

Perry, R. P. and Kelley, D. E. (1970). Inhibition of RNA synthesis by actinomycin D: characteristic dose-response of different RNA species. *J. Cell. Physiol.* **76**, 127–139.

Potapova, T. A. and Gerton, J. L. (2019). Ribosomal DNA and the nucleolus in the context of genome organization. *Chromosome Res.* **27**, 109–127.

Probst, A. V., Santos, F., Reik, W., Almouzni, G. and Dean, W. (2007). Structural differences in centromeric heterochromatin are spatially reconciled on fertilisation in the mouse zygote. *Chromosoma* **116**,.

Probst, Aline. V., Okamoto, I., Casanova, M., El Marjou, F., Le Baccon, P. and Almouzni, G. (2010). A Strand-Specific Burst in Transcription of Pericentric Satellites Is Required for Chromocenter Formation and Early Mouse Development. *Dev. Cell* **19**, 625–638.

Romanova, L. (2006). High Resolution Mapping of Ribosomal DNA in Early Mouse Embryos by Fluorescence In Situ Hybridization. *Biol. Reprod.* **74**, 807–815.

Sanij, E., Hannan, K. M., Xuan, J., Yan, S., Ahern, J. E., Trigos, A. S., Brajanovski, N., Son, J., Chan, K. T., Kondrashova, O., et al. (2020). CX-5461 activates the DNA damage response and demonstrates therapeutic efficacy in high-grade serous ovarian cancer. *Nat. Commun.* **11**, 2641.

Savić, N., Bär, D., Leone, S., Frommel, S. C., Weber, F. A., Vollenweider, E., Ferrari, E., Ziegler, U., Kaech, A., Shakhova, O., et al. (2014). lncRNA Maturation to Initiate Heterochromatin Formation in the Nucleolus Is Required for Exit from Pluripotency in ESCs. *Cell Stem Cell* **15**, 720–734.

Schindelin, J., Arganda-Carreras, I., Frise, E., Kaynig, V., Longair, M., Pietzsch, T., Preibisch, S., Rueden, C., Saalfeld, S., Schmid, B., et al. (2012). Fiji: an open-source platform for biological-image analysis. *Nat. Methods* **9**, 676–682.

Schindelin, J., Rueden, C. T., Hiner, M. C. and Eliceiri, K. W. (2015). The ImageJ ecosystem: An open platform for biomedical image analysis. *Mol. Reprod. Dev.* **82**, 518–529.

Schneider, C. A., Rasband, W. S. and Eliceiri, K. W. (2012). NIH Image to ImageJ: 25 years of image analysis. *Nat. Methods* **9**, 671–675.

Schöfer, C., Weipoltshammer, K., Almeder, M., Müller, M. and Wachtler, F. (1996). Redistribution of ribosomal DNA after blocking of transcription induced by actinomycin D. *Chromosome Res.* **4**, 384–391.

Shishova, K. V. and others (2011). The fate of the nucleolus during mitosis: comparative analysis of localization of some forms of pre-rRNA by fluorescent in situ hybridization in NIH/3T3 mouse fibroblasts. *Acta Naturae Англоязычная Версия* **3**,.

Shishova, K. V., Lavrentyeva, E. A., Dobrucki, J. W. and Zatsepina, O. V. (2015a). Nucleolus-like bodies of fully-grown mouse oocytes contain key nucleolar proteins but are impoverished for rRNA. *Dev. Biol.* **397**, 267–281.

Shishova, K. V., Khodarovich, Y. M., Lavrentyeva, E. A. and Zatsepina, O. V. (2015b). High-resolution microscopy of active ribosomal genes and key members of the rRNA processing machinery inside nucleolus-like bodies of fully-grown mouse oocytes. *Exp. Cell Res.* **337**, 208–218.

Solovei, I., Kreysing, M., Lanctôt, C., Kösem, S., Peichl, L., Cremer, T., Guck, J. and Joffe, B. (2009). Nuclear Architecture of Rod Photoreceptor Cells Adapts to Vision in Mammalian Evolution. *Cell* **137**, 356–368.

Stalling, D., Westerhoff, M. and Hege, H.-C. Amira - a Highly Interactive System for Visual Data Analysis. 18.

Stefanovsky, V. Y., Pelletier, G., Bazett-Jones, D. P., Crane-Robinson, C. and Moss, T. (2001). DNA looping in the RNA polymerase I enhancesome is the result of non-cooperative in-phase bending by two UBF molecules. *Nucleic Acids Res.* **29**, 3241–3247.

Szabo, Q., Donjon, A., Jerković, I., Papadopoulos, G. L., Cheutin, T., Bonev, B., Nora, E. P., Bruneau, B. G., Bantignies, F. and Cavalli, G. (2020). Regulation of single-cell genome organization into TADs and chromatin nanodomains. *Nat. Genet.* **52**, 1151–1157.

Therizols, P., Illingworth, R. S., Courilleau, C., Boyle, S., Wood, A. J. and Bickmore, W. A. (2014). Chromatin decondensation is sufficient to alter nuclear organization in embryonic stem cells. *Science* **346**, 1238.

van de Nobelen, S., Rosa-Garrido, M., Leers, J., Heath, H., Soochit, W., Joosen, L., Jonkers, I., Demmers, J., van der Reijden, M., Torrano, V., et al. (2010). CTCF regulates the local epigenetic state of ribosomal DNA repeats. *Epigenetics Chromatin* **3**, 19.

van Sluis, M. and McStay, B. (2017). Nucleolar reorganization in response to rDNA damage. *Curr. Opin. Cell Biol.* **46**, 81–86.

van Steensel, B. and Furlong, E. E. M. (2019). The role of transcription in shaping the spatial organization of the genome. *Nat. Rev. Mol. Cell Biol.* **20**, 327–337.

Wang, Q. T., Piotrowska, K., Ciemerych, M. A., Milenkovic, L., Scott, M. P., Davis, R. W. and Zernicka-Goetz, M. (2004). A Genome-Wide Study of Gene Activity Reveals Developmental Signaling Pathways in the Preimplantation Mouse Embryo. *Dev. Cell* **6**, 133–144.

West, J. (1995). Manipulating the Mouse Embryo . A Laboratory Manual, 2nd Edition. By Brigid Hogan, Rosa Beddington, Frank Costantini and Elizabeth Lacy. Cold Spring Harbor Laboratory Press 1994, 497 pages. Price $95. ISBN 0-87969-384-3.--- Either ISSN or Journal title must be supplied.

Yao, R.-W., Xu, G., Wang, Y., Shan, L., Luan, P.-F., Wang, Y., Wu, M., Yang, L.-Z., Xing, Y.-H., Yang, L., et al. (2019). Nascent Pre-rRNA Sorting via Phase Separation Drives the Assembly of Dense Fibrillar Components in the Human Nucleolus. *Mol. Cell* **76**, 767-783.e11.

Yu, M. and Ren, B. (2017). The Three-Dimensional Organization of Mammalian Genomes. *Annu. Rev. Cell Dev. Biol.* **33**, 265–289.

Zatsepina, O., Baly, C., Chebrout, M. and Debey, P. (2003). The Step-Wise Assembly of a Functional Nucleolus in Preimplantation Mouse Embryos Involves the Cajal (Coiled) Body. *Dev. Biol.* **253**, 66–83.

Zentner, G. E., Balow, S. A. and Scacheri, P. C. (2014). Genomic Characterization of the Mouse Ribosomal DNA Locus. *G3amp58 GenesGenomesGenetics* **4**, 243–254.

Figures

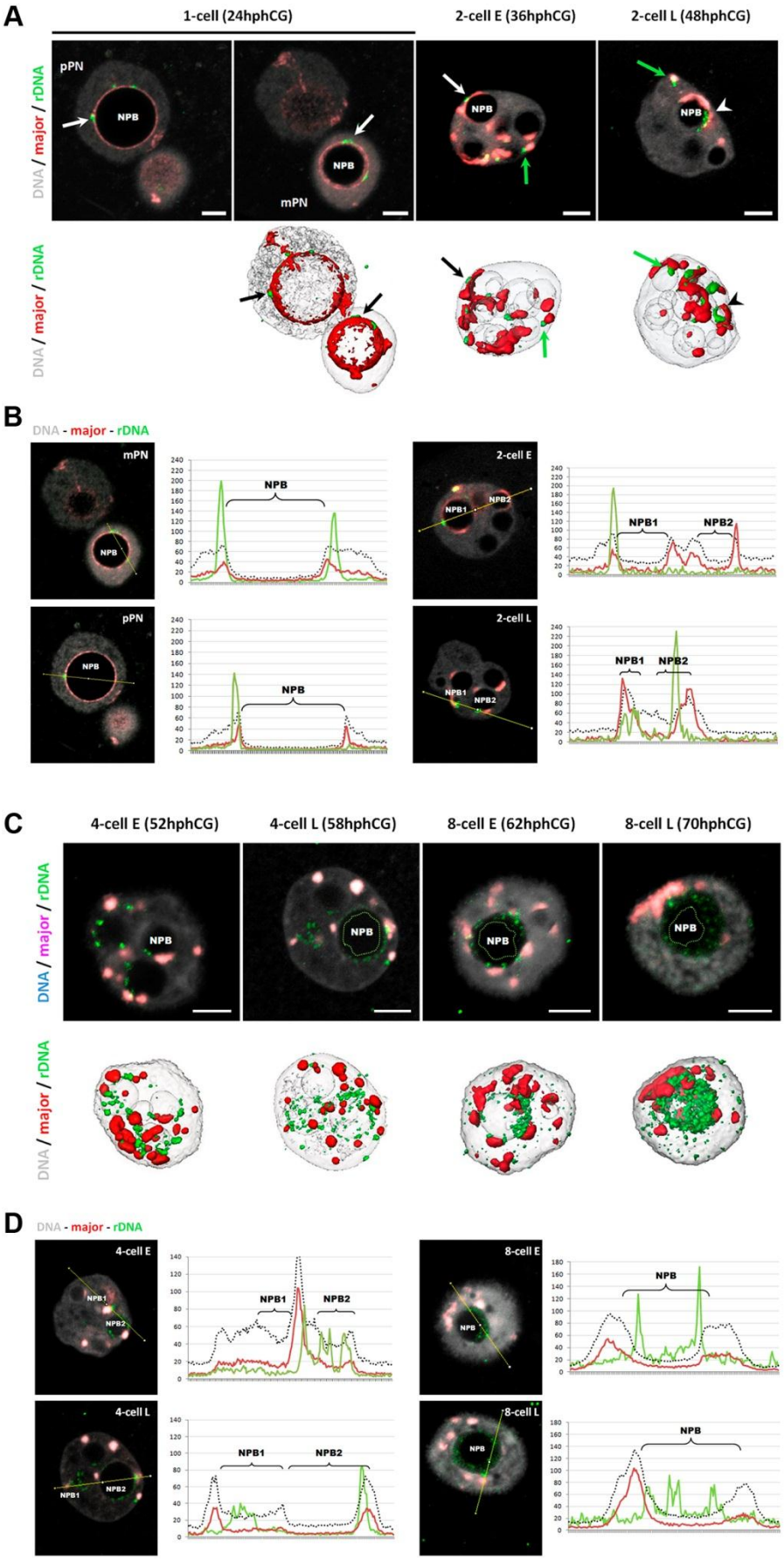

Figure 1: **3D organization of ribosomal sequences (rDNA) is correlated with their transcriptional state**

(A) 3D organization of rDNA and major satellite sequences at 1-cell and 2-cell stages detected by 3D DNA-FISH using specific probes. Upper panel : single z-section of a representative nucleus of 1-cell (24hphCG, z=30/68 and 43/68 for pPN and mPN respectively), early (E, 36hphCG, z=29/74) and late (L, 48hphCG, z=26/69) 2-cell stages. Lower panel: Amira 3D representation of each nucleus. White (or black, lower panel) arrows indicate clustered rDNA FISH signal juxtaposed to major satellite signal at NPBs surface; green arrows indicated rDNA juxtaposed to round shape major satellite signal and white (or black, lower panel) arrowhead indicate pearl necklace rDNA signal at NPBs surface. **(B)** Localization of rDNA and major satellite signals in regards to NPBs boundaries at 1-cell and 2-cell stages. Left panel: single z-section of the nucleus with the line corresponding to the Intensity profile measurement in Fiji. Right panel: Fluorescence intensity plot profile along the line (chosen to cross at least one NPB and also major satellite and rDNA signals) for the three channels (dark dotted line for DNA, green line for rDNA signal, and red line for major satellite signal, x axis corresponds to the pixel poition of in the image and y axis corresponds to the intensity of fluorescence). **(C)** 3D organization of rRNA genes at 4-cell and 8-cell stages detected by 3D DNA-FISH. rDNA FISH signal expands in the inner of the NPBs up to fulfil it completely. Upper panel: z-section of a representative nucleus of early (E) or late (L) 4-cell and 8-cell stage. Lower panel: Amira 3D representation of each nucleus. **(D)** Localization of rDNA and major satellite signals with regard to NPBs boundaries at 4-cell and 8-cell stages. Left panel: single z-section of the nucleus with the line corresponding to the Intensity profile measurement in Fiji. Right panel: Fluorescence intensity plot profile along the line across multiple channels (blue dot line for DAPI, the green line for rDNA signal, and red line for major satellite signal). *Scale bar = 5µm*. mPN: maternal Pronucleus; pPN : paternal Pronucleus and NPB: Nucleolar Precursor Body; h phCG : hours post-injection of human Chorionic Gonadotrophin, major: mouse major satellite sequences, rDNA: ribosomal DNA.

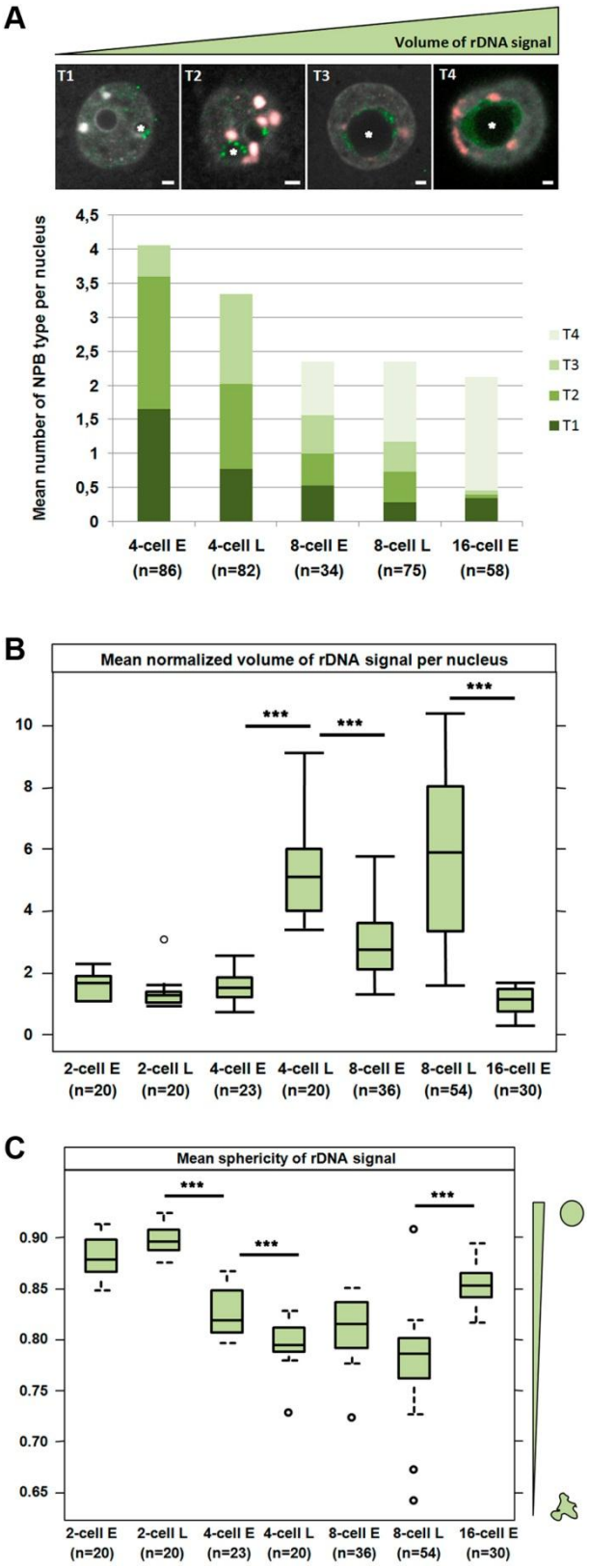

Figure 2: Features of rDNA spatial organization during pre-implantation development

(A) Spatial organization rDNA surrounding the NPBs. Upper panel: Four kinds of NPBs can be defined depending on their rDNA pattern: Type 1 (T1) displays small dots of rDNA signal,

Type 2 (T2) shows spots distributed like a pearl necklace, Type 3 (T3) harbors a thin cloud of rDNA signal and Type 4 (T4) a large cloud of rDNA signal. Stars indicated the NPBs representative of each type. Scale bar = 5µm. Lower panel: Quantification of the number of each type of rDNA/NPBs pattern per stage at the 4-cell, 8-cell (early (E) and late (L)) and the early 16-cell stage. Mann-Whitney test was used to compare (two by two) the distribution of the type between stages. **, p-value< 0.01; ***, p-value < 0.001. **(B and C)** Quantification of rDNA total volume (B) and average sphericity (C) per nucleus and stage based on the DNA-FISH signal of the ribosomal sequences. All measurements were done using Imaris 9.6 (Oxford Instruments) from the 2-cell to 16-cell stage. Statistical significance was evaluated using a non-parametric multiple comparison test (nparcomp, R package). ***, p-value < 0.001. The number of nuclei examined per stage is indicated below the stage name.

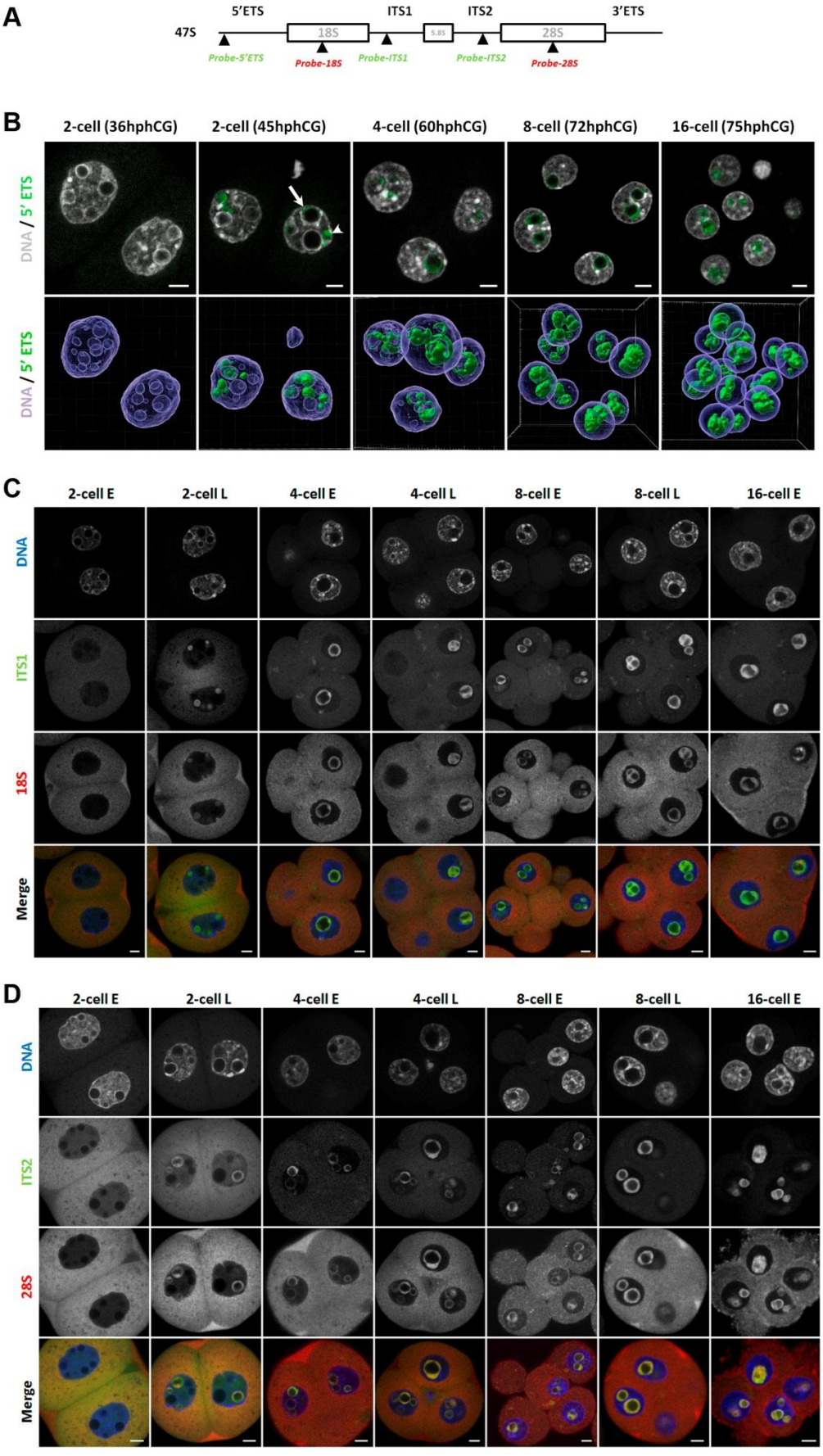

Figure 3: **rRNA transcripts organization upon early development**

(A) Schematic representation of the rDNA sequence and position of the rRNA FISH probes used in this study. Each repeat of the mouse ribosomal sequence (X 82564.1) is transcribed in a long mRNA (47S) encoding for 18S, 5.8S, and 28S rRNAs, separated by two external transcribed spacers (5'ETS and 3'ETS) and two internal transcribed spacer (ITS1 and ITS2). **(B)** rDNA transcripts (green) are visualized by RNA-FISH using a specific probe for the 5'ETS region. Upper panel: representative nuclei of 2-cell (36h and 45hphCG), 4-cell (60hphCG), 8-cell (72hphCG) and 16-cell (75hphCG) stages embryos. Arrow indicates immature rRNA labeled with a 5'ETS probe at the surface of an NPB and arrowhead indicates immature rRNA outside NPB. Lower panel: 3D representation of a whole embryo at each stage using Imaris 9.6 for channel segmentation. DNA is labeled in grey and rDNA transcripts in green. *Scale bar = 5µm*. **(C and D)** Single z-section (from confocal stack images) of a representative nuclei from 2-cell (early (E) and late (L)), 4-cell (early (E) and late (L)), 8-cell (early (E) and late (L)) and early 16-cell stages embryos. Specific oligonucleotides of respectively **(C)** the Internal transcribed spacer 2 (ITS2) and the 28S rRNA sequences and **(D)** the Internal transcribed spacer 1 (ITS1) and the 18S rRNA sequences were used to visualize pre-rRNA processing regions in the nucleoli of mouse embryos nuclei by RNA-FISH. As the 28S and 18S rRNA probes are also labeled the ribosomes, the cytoplasm is labeled with these probes. DNA is in blue, ITS2 and ITS1 rRNAs are in green, and 18S and 28S rRNAs are in red. *Scale bar = 5µm*.

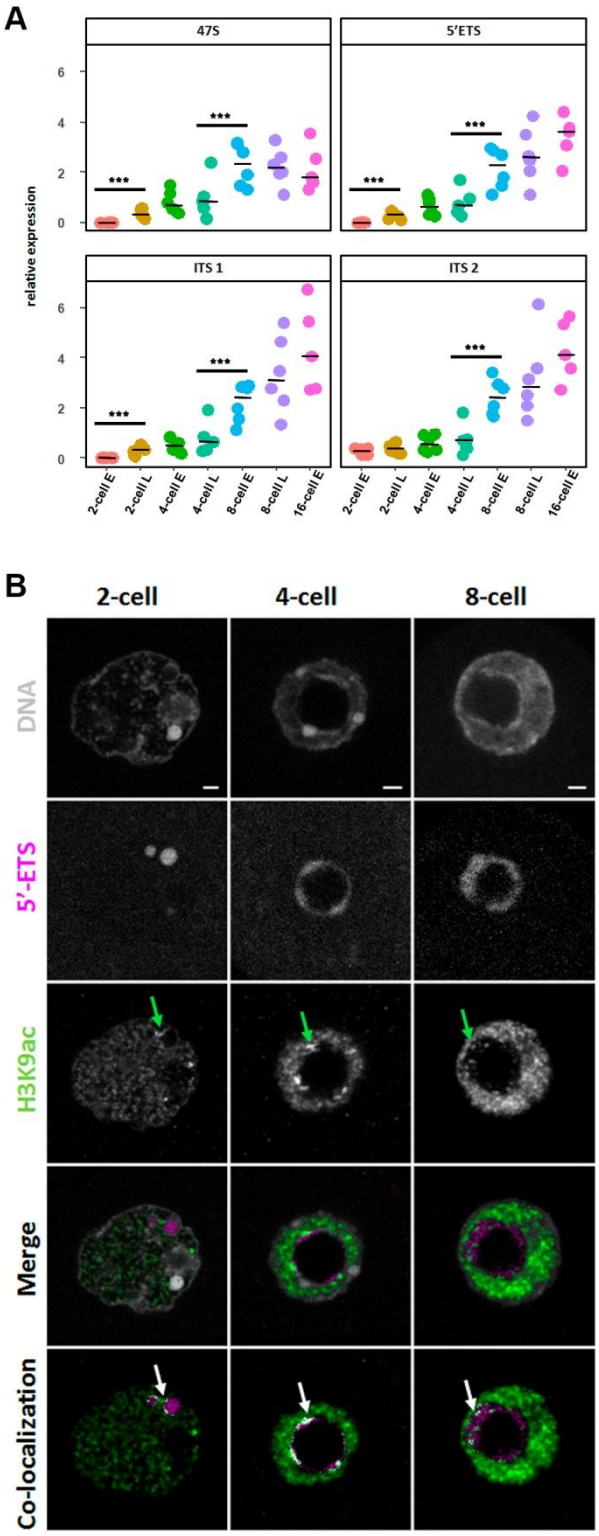

Figure 4: **rRNA transcripts amount and localization euchromatine epigenetics marks**

(A) Quantification of the rRNA transcription at 2-cell (early (E) and late (L)), 4-cell (e and L), 8-cell (E and L), and 16 cell stages by Real-Time qPCR (RT-qPCR) using primers (described in Table S2) specific of 47S long pre-rRNA, of 5'ETS, ITS1 and ITS2 regions. Four to six biological replicates were done by stage, the expression of these pre-RNA was normalized to

a fixed amount of luciferase mRNA added before the reverse transcription. Statistical significance was evaluated using a non-parametric multiple comparison test (nparcomp, R package). ***, p-value < 0.001. **(B)** Localization of H3K9ac (green) and immature rRNA (magenta) by immuno-RNA-FISH from 2-cell to 8-cell stage. Green arrows indicate H3K9ac bright and big foci close or inside the 5'ETS RNA-FISH signal. Pixels (point by white arrows) that correspond to co-localization between H3K9ac and 5'ETS fluorescent channels were identified using Imaris 9.6 software.

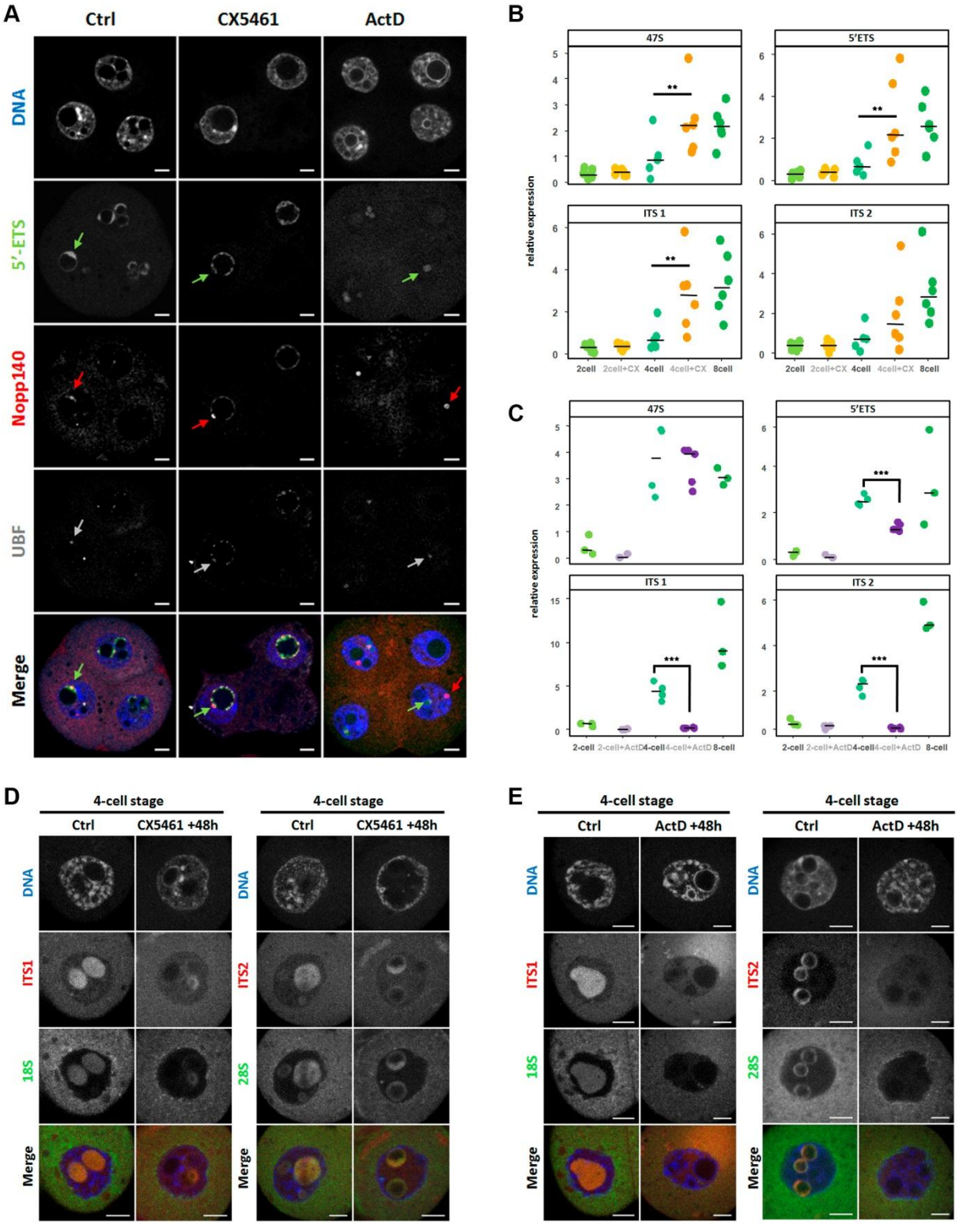

Figure 5: **Inhibition of rRNA transcription by CX-5461 and ActD**.

(A) Localization using immuno RNA-FISH of nascent rRNA (5'ETS probe in green), Nopp140 (red) and UBF (grey) at 4-cell stage in non treated (Ctrl) and treated embryos (CX-5461 and ActD), nuclei were counterstained with DAPI (blue). Every single z-section of a

confocal stack image show representative nuclei. Green arrows point 5'ETS FISH signals, red arrows Nopp140 immunostaining, and grey arrows UBF immunostaining. *Scale bar = 5µm.* **(B and C)** Quantification by RT-qPCR of the relative expression of rRNAs amplified with specific primers for 47S, 5'ETS, ITS1, and ITS2 in control embryos (2-cell, 4-cell and 8 cell stages, green spots) and treated embryos (2-cell and 4-cell stages): with CX-5461 (B, orange spots) and actinomycin D (C, purple spots). Statistical significance between control and treated embryos was evaluated using the Mann-Whitney test (wilcox, R-package). *, p-value < 0.05, **, p-value < 0.01. **(D and E)** Representative confocal images of 4-cell stages nuclei in non-treated (Ctrl) and treated embryos with CX-5461 (D) or Actinomycin D (E). In process pre-rRNAs species were localized by RNA-FISH with specific fluorescent oligoprobes for ITS1 (red) - 18S (green), left panel or ITS2 (red) - 28S (green), right panel. Nuclei were counterstained with DAPI (blue). *Scale bar = 5µm.*

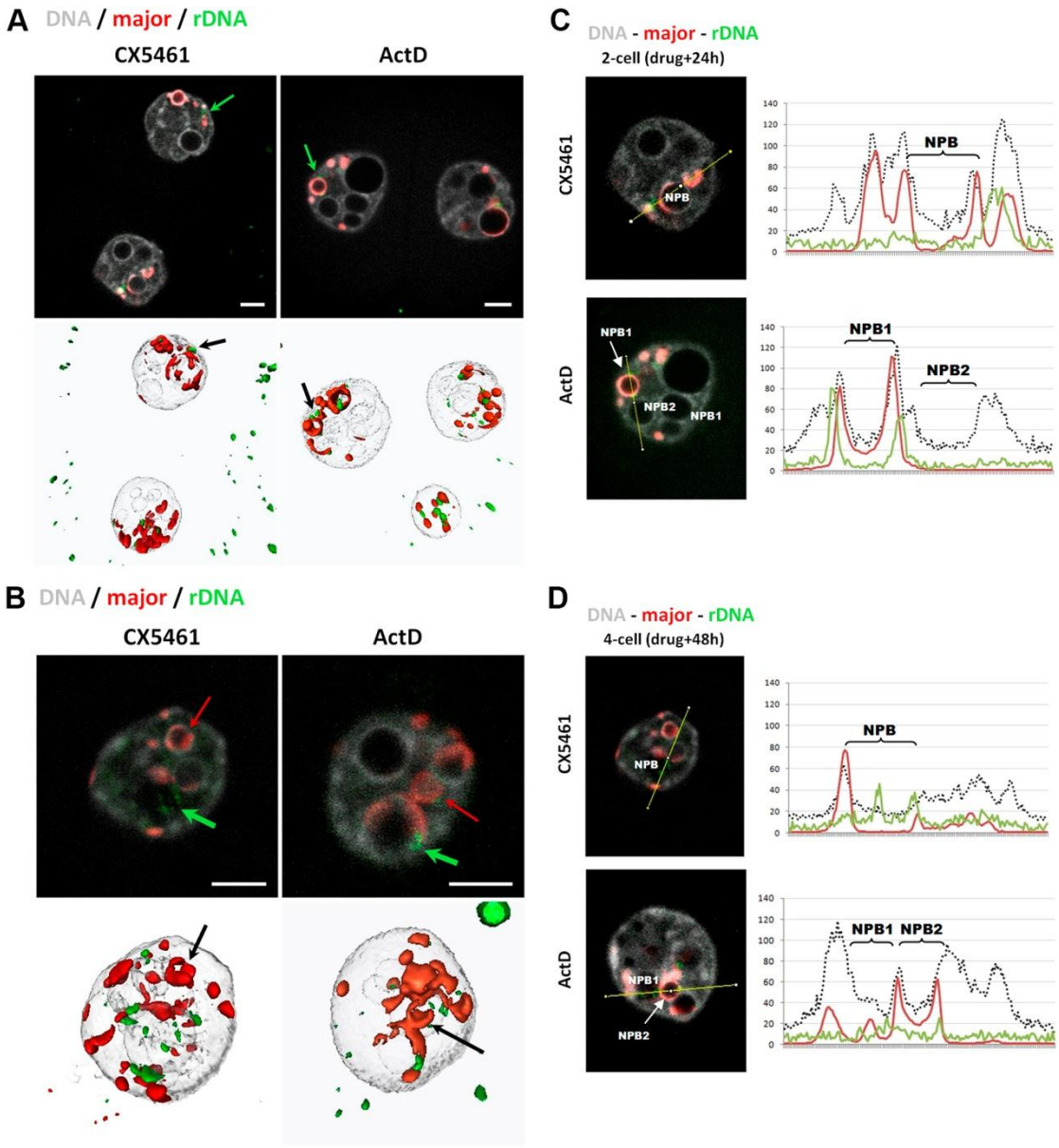

Figure 6: **Consequences of rRNA synthesis Inhibition on the spatial organization of ribosomal sequences**

(A) 3D organization of rDNA and major satellite sequences at 2-cell stages detected by 3D DNA-FISH using specific probes. Upper panel: single z-section of representative nuclei of non-treated (Ctrl) and treated embryos (CX-5461 and ActD). Lower panel: Amira 3D representation of 2-cell embryos. Green arrows indicate clustered rDNA FISH signal juxtaposed to major satellite signal at NPBs surface **(B)** 3D organization of rDNA and major satellite sequences at 4-cell stages detected by 3D DNA-FISH. Upper panel: single z-section of representative nuclei of non-treated (Ctrl) and treated embryos (CX-5461 and ActD). Lower panel: Amira 3D representation of each embryo. Green arrows indicate clustered rDNA FISH signal and red arrows major satellite sequences FISH signal with a ring/half-ring

shape. Black arrow point major satellite sequences FISH signal with a round shape called chromocenter. **(C and D)** Localization of rDNA and major satellite signals in regards to NPBs boundaries at 2-cell stage (C) and 4-cell stage (D) in non-treated (Ctlr) and treated (CX-5461 or ActD) embryos. Left panel: single z-section of a representative nucleus with the line used to draw with Fiji the Intensity plot profile. Right panel: Fluorescence intensity plot profile along the line across multiple channels (Dark dotted line for DAPI, green line for rDNA signal, and red line for major satellite signal). DNA is in grey, rDNA in green, and major satellite sequences in magenta. *Scale bar = 5µm*. Major : mouse major satellite sequences, rDNA: ribosomal DNA.

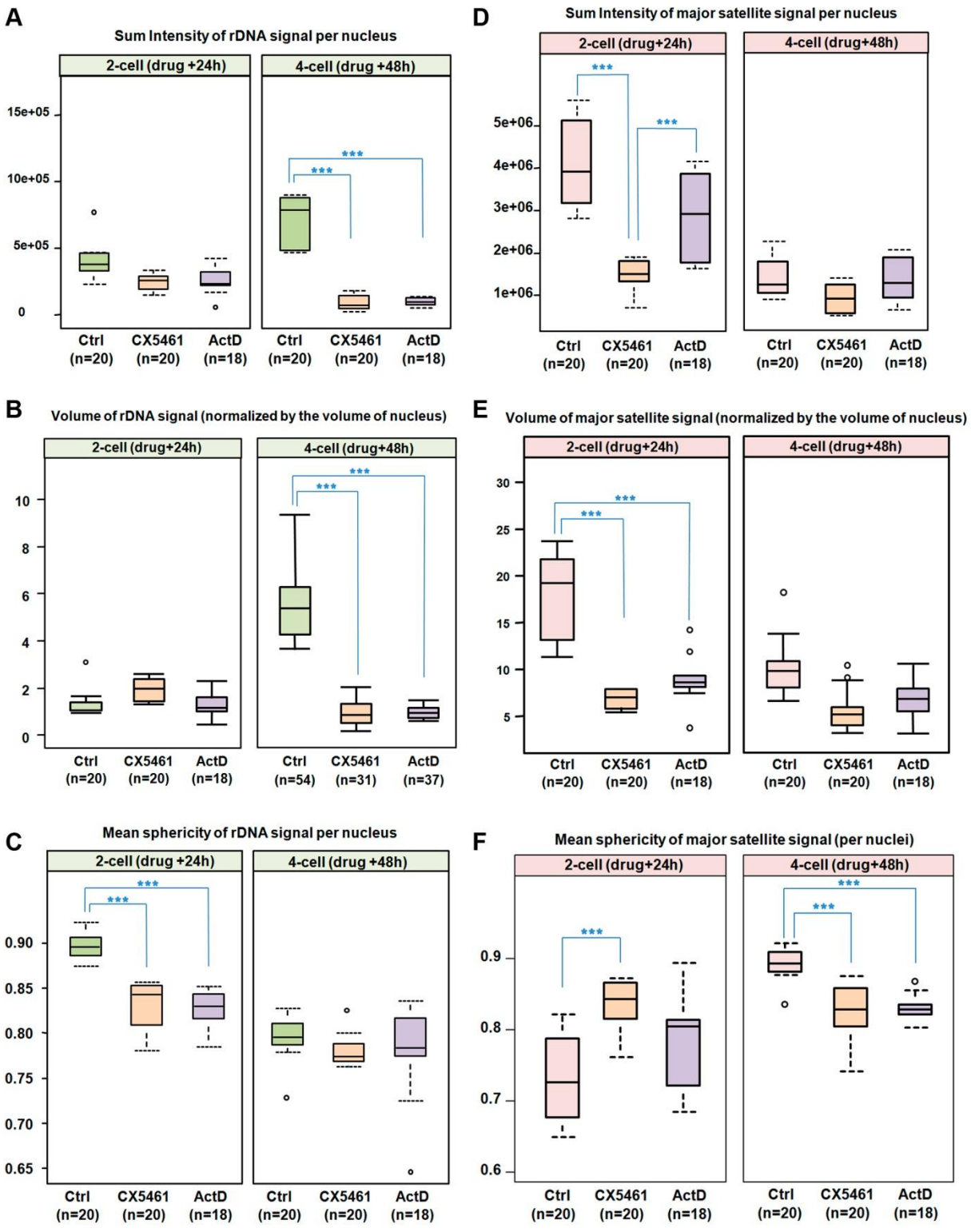

Figure 7: **Consequences of rRNA synthesis Inhibition on rDNA and major satellite sequences 3D conformation.**

(A, B and C) Quantification of rDNA Sum of Intensity (A), total volume (B) and average sphericity (C) per nucleus and stage based on the DNA-FISH signal of the ribosomal sequences at 2-cell and 4-cell stages in non-treated (Ctrl) and treated (CX-5461 or ActD)

embryos. The number of nuclei examined per condition is indicated below the name of the condition (Ctrl in green, CX-5461 in orange, and ActD in purple). **(D, E and F)** Quantification of major satellite sequence Sum of Intensity (D), total volume (E) and average sphericity (F) per nucleus and per stage based on the DNA-FISH signal, at 2-cell and 4-cell stages in non-treated (Ctrl) and treated (CX-5461 or ActD) embryos. The number of nuclei examined per condition is indicated below the name of the condition (Ctrl in pink, CX-5461 in orange, and ActD in purple). All measurements were done using Imaris 9.6 (Oxford Instruments). Statistical significance was evaluated using a non-parametric multiple comparison test (nparcomp, R package). ***, p-value < 0.001.

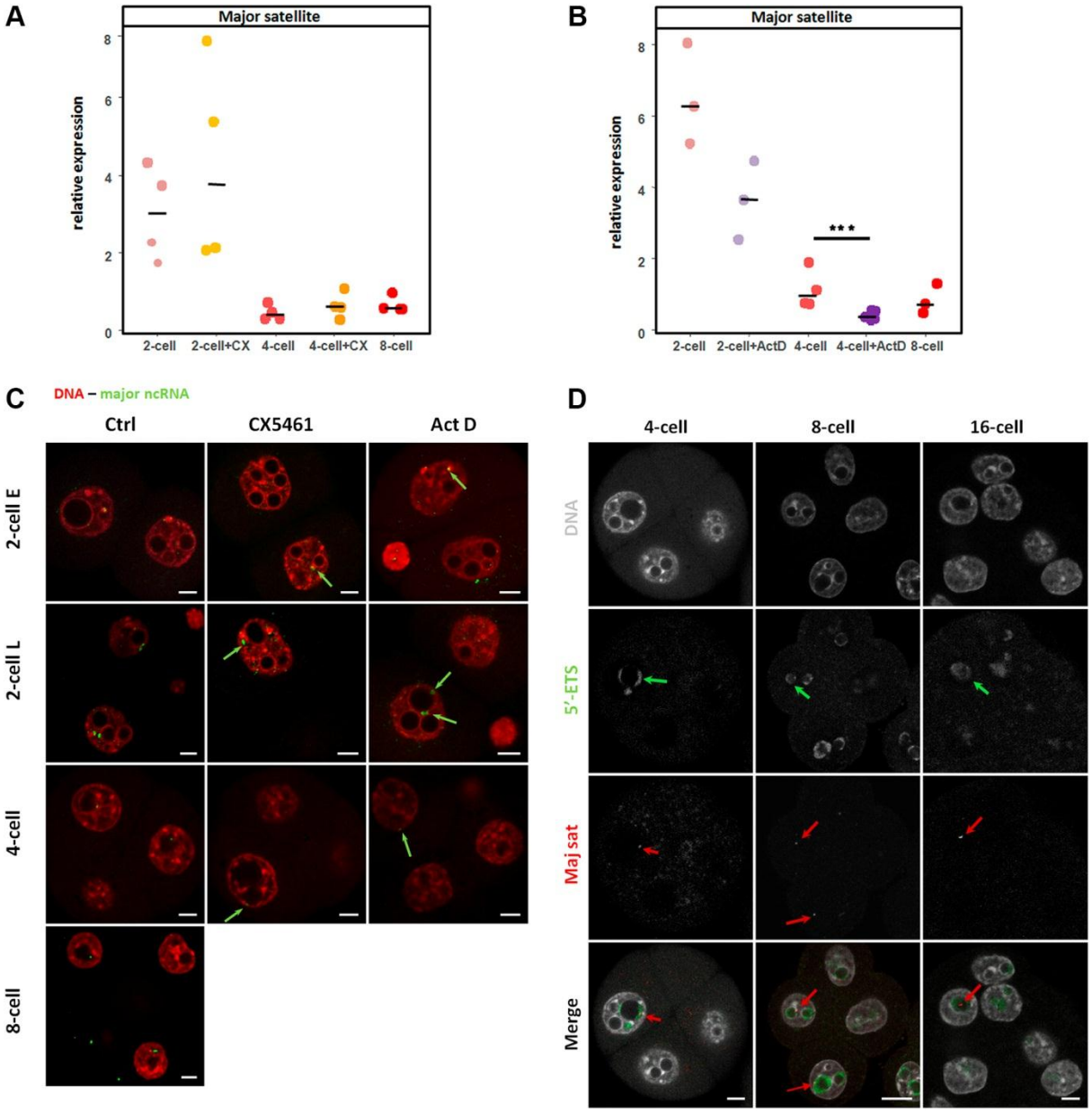

Figure 8: Consequences of rRNA synthesis Inhibition on the expression of major satellite sequences

(A and B) Quantification by RT-qPCR of the relative expression of ncRNA amplified with specific primers for major satellite sequence in control embryos (2-cell, 4-cell and 8 cell stages, pink/red spots) and treated embryos (2-cell and 4-cell stages): with CX-5461 (A, orange spots) and actinomycin D (B, purple spots). Statistical significance between control and treated embryos was evaluated using the Mann-Whitney test (Wilcox, R-package). **, p-value < 0.01. **(C)** Major satellite transcripts (green) visualized using RNA-FISH in non treated (Ctlr) in non-treated (Ctrl) and treated (CX-5461 or ActD) embryos from 2-cell (early (E) and late (L)) to 4-cell and 8-cell stages. ncRNAs spots are indicated by green arrows in

treated embryos, DAPI is in red. **(D)** Localization of immature rRNAs (green) and major satellite ncRNAs (red) in mouse embryos from the 4-cell to 16-cell stages by RNA-FISH using specific probes for 5'ETS region and major satellite sequences. Green arrows indicate a 5'ETS RNA-FISH signal closed to a major satellite signal (red arrows). Nuclei were counterstained with DAPI (grey). *Scale bar = 5µm*.

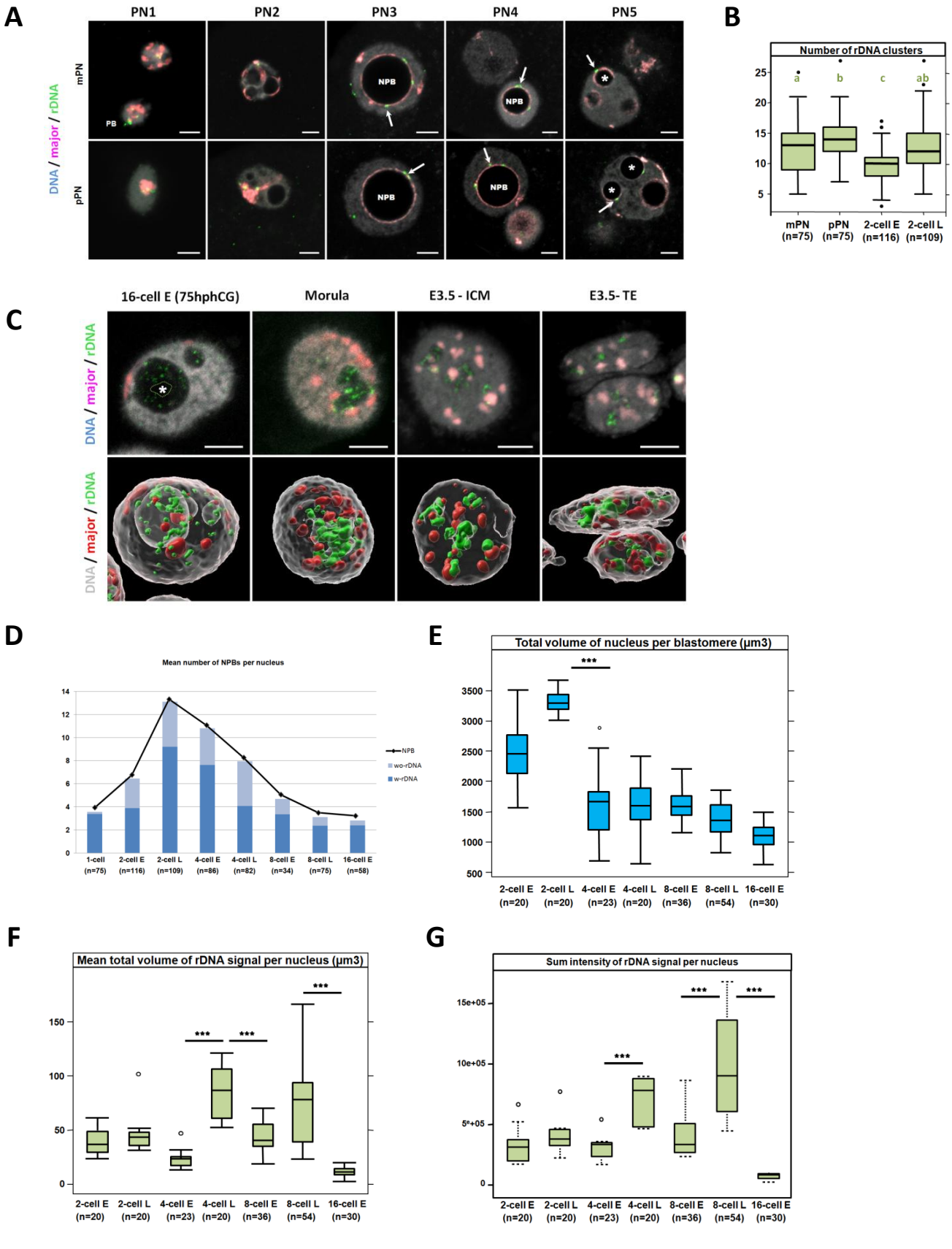

Fig. S1. 3D organization of ribosomal sequences (rDNA) is correlated with their transcriptional state
(A) 3D organization of rDNA and major satellite sequences at 1-cell. Single z-section of Paternal (pPN) and maternal (mPN) of the same 1-cell embryo are shown separately at the different pronuclei stages (PN1 to PN5) according to (Adenot et al., 1997). Arrows indicate clusters of rDNA associated with major satellite sequences. rDNA is located at Nucleolar Precursor bodies surface (indicated by "NPB" or by a star) from PN3 to PN5. DNA is in blue, rDNA in green, and major sat sequences in magenta. *Scale bar = 5µm.*
(B) Quantification of the mean number of rDNA cluster at 1-cell to 2-cell stages.
(C) 3D organization of rDNA from 16-cell to Blastocyste stages detected by 3D-DNA FISH. Upper panel: z-section of a representative nucleus at 16-cell and morula stages and also at Blastocyst stage 3.5 days after fertilization (E3.5) in the inner cell mass (ICM) and the trophectoderm (TE). Lower panel: Imaris representation in 3D of the same nucleus. DNA is in blue or grey, rDNA in green, and major satellite sequences in magenta. *Scale bar = 5µm.*
(D) Quantification of the total number of NPBs (black line) and the ones that are associated (dark blue bars) with rDNA sequences or not associated (blue bars) from the 1-cell up to the 16-cell stage. The early stage is indicated by (E) and the late one by (L).
(E, F and G) Measurement of the total volume (µm3) of the nucleus **(E)** and quantification of the total volume (µm3) and the sum of the intensities of the DNA-FISH signal for the ribosomal sequences **(F and G)** at the 2-cell to 16-cell stage. All measurements were done using Imaris 9.6 (Oxford Instruments). Statistical significance was evaluated using a non-parametric multiple comparison test (nparcomp, R package). ***, p-value < 0.001.

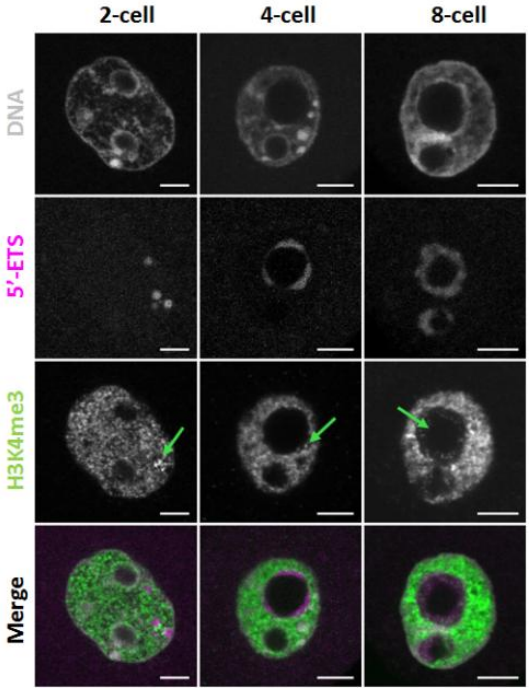

Fig. S2. Localization of H3K4me3 and immature transcripts of rRNA by immunoRNA-FISH

Localization of H3K4me3 (green) and nascent rRNA (magenta) by immuno-RNA-FISH from 2-cell to 8-cell stage. Green arrows indicate H3K4me3 foci close or inside the 5'ETS RNA-FISH signal. DNA is in gray. *Scale bar = 5µm.*

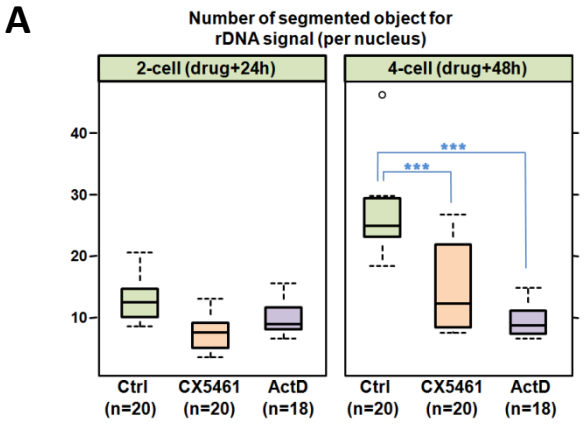

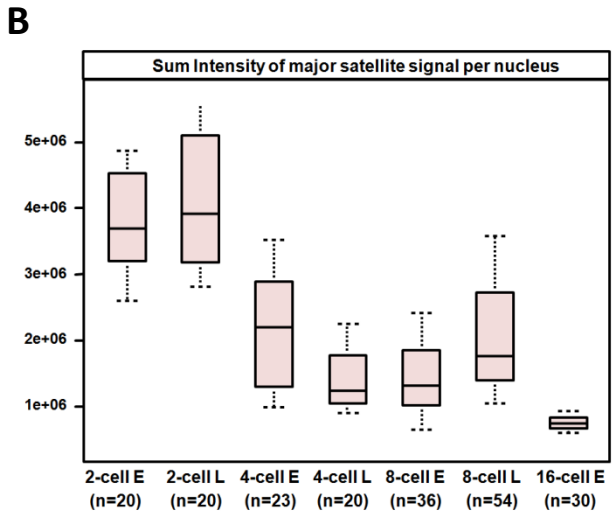

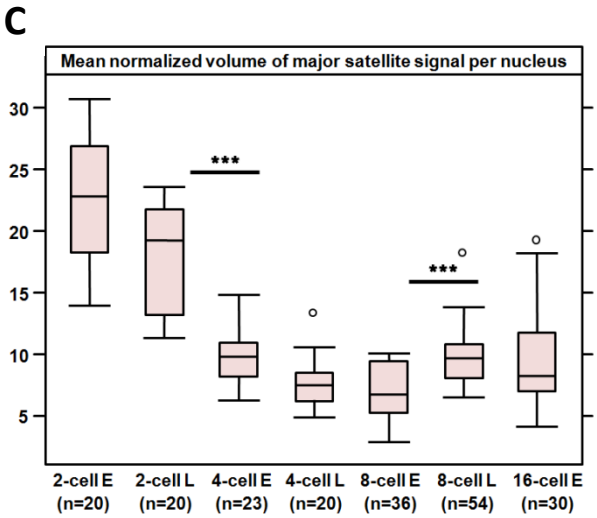

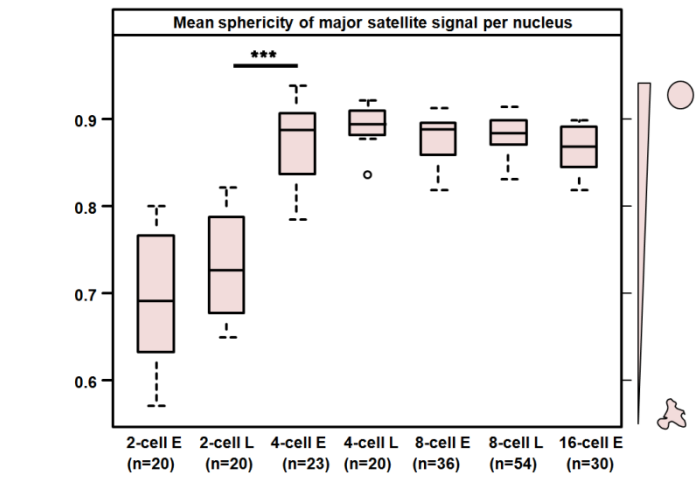

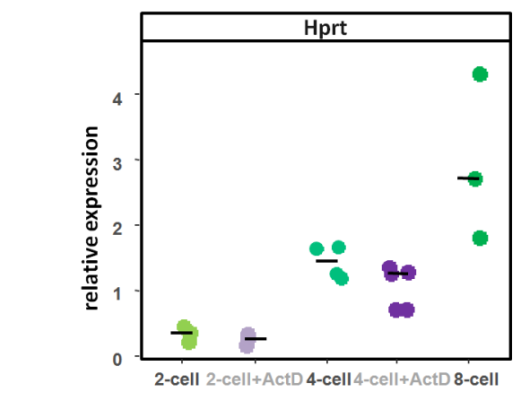

Fig. S3. Quantification of several parameters of segmented objects and relative expression of an housekeeping gene (Hprt)

(A) Quantification of mean number of rDNA objects in control and treated embryos based on the DNA-FISH signal,

(B, C and D) Quantification of the sum of the intensity **(B)**, total volume **(C)** and average sphericity **(D)** per nucleus and per stage based on the major satellite sequence DNA-FISH signal, from 2-cell up to 16-cell stage embryos. The number of nuclei examined per stage is indicated below the name of the stage. All measurements were done using Imaris 9.6 (Oxford Instruments). Statistical significance was evaluated using a non-parametric multiple comparison test (nparcomp, R package). ***, p-value < 0.001.

(E) Quantification by RT-qPCR of the relative expression of mRNA amplified with specific primers for Hprt sequence in non-treated (Ctrl) embryos (2-cell, 4-cell, and 8 cell stages, green spots) and treated (ActD) embryos (2-cell and 4-cell stages, purple spots). Three to four biological replicates were done by condition, the amount of transcript was normalized to a fixed amount of Luciferase added before the reverse transcription according to previous protocol (Bui et al 2009).

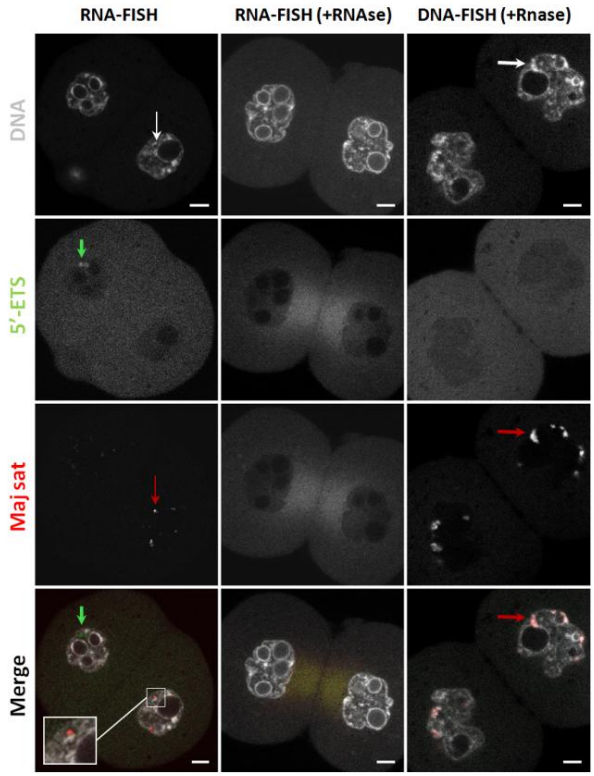

Fig. S4. RNA-FISH of 5'ETS and major satellite specific probes

A positive control of the RNA-FISH procedure is showed in the first panel. The magnification focus on a major satellite signal that is close to a bright DAPI foci.
The middle panel correspond to the negative control with embryos incubated with RNase before the RNA-FISH procedure.
The last panel allows the comparison between major satellite DNA-FISH signals (red arrow in last panel) and major satellite RNA-FISH signals (red arrow in first panel).
The DNA is in gray, the 5'ETS signal in green and the major satellite signal in red. *Scale bar = 5µm.*

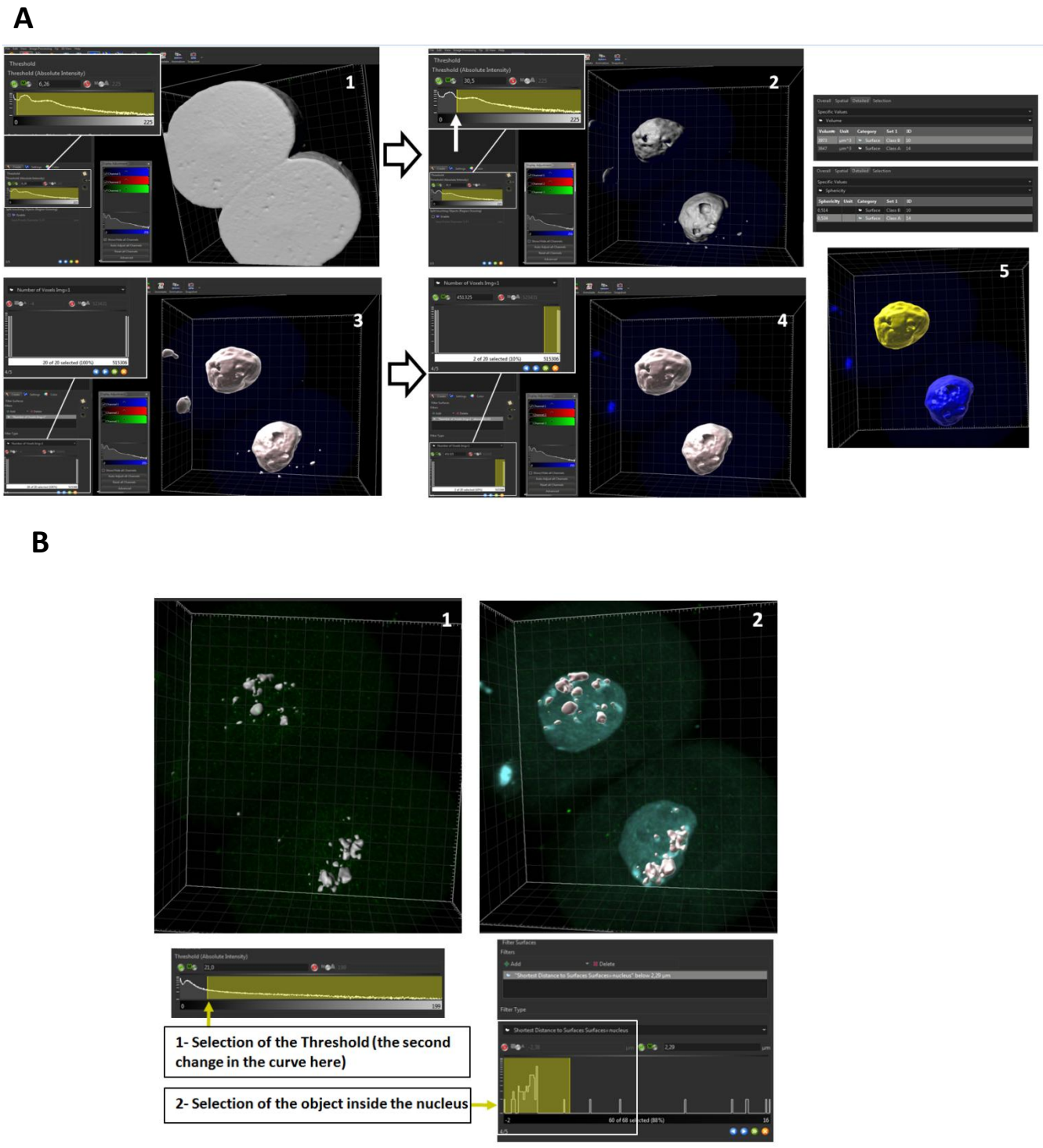

Fig. S5. Description of the workflow used to segment DNA and rDNA the images.
Segmentation workflow of the nucleus **(A)** and the rDNA FISH signal **(B)** using "Surface" module of Imaris 9.6 (Bitplane). **(A)** The white arrow indicate the threshold proposed by the wizard option in the first step of the segmentation process (1 and 2). The second step allow chosing the size of the object (3 and 4); At the last step (5), labeled objects can be selected to measure several parameters (here the volume and the sphericity). Magnifications show the theshold window. **(B)** The same procedure is applied to rDNA FISH signal except that Imaris allows selection of objects with regards to the distance of labeled objects in other channels (for instance nucleus).

Table S1. List and sequence of the probes used for the RNA-FISH experiments

Name	Sequence	Fluorophore in 5'	Position from TSS	Position in X82564.1
5'ETS	AGA-GAA-AAG-AGC-GGA-GGT-TCG-GGA-CTC-CAA	Alexa-488	346-375	5981-6010
ITS1	TAG-ACA-CGG-AAG-AGC-CGG-ACG-GGA-AAG-A	Cy3	6135-6163	11770-11798
ITS2	CCA-GCG-CAA-GAC-CCA-AAC-ACA-CAC-AGA	Cy3	7496-7523	13131-13158
18S	CCA-TTA-TTC-CTA-GCT-GCG-GTA-TCC-AGG-CGG	Cy5	4849-4876	10484-10511
28S	GAG-GGA-ACC-AGC-TAC-TAG-ATG-GTT-CGA-TTA	Cy5	9573-9600	15208-15235
major-LNA-sense	6A6-A6T-8T5-G7A-6G8-G5A	Cy3		

Table S2. List and sequence of the primers used for the RT-qPCR experiments

Name	Sense	Sequence (5'->3')	References
47S - F	forward	GGTGTCCAAGTGTTCATG	From (Fulka and Langerova, 2014)
47S - R	reverse	CAAGCGAGATAGGAATGTCTTAC	
5'ETS - F	forward	TGTTTCACTTTGGTCGTGTCTC	From (Fulka and Langerova, 2014)
5'ETS - R	reverse	TCGACGCTTACAAGAAACAGC	
ITS1 - F	forward	TCTCGTTTCGTTCCTGCTGG	From (Fulka and Langerova, 2014)
ITS1 - R	reverse	GATCCACCGCTAAGAGTCGTATC	
ITS2 - F	forward	CGTGTGAGTAAGATCCTCCAC	From (Fulka and Langerova, 2014)
ITS2 - R	reverse	GTTACTGAGGGAATCCTGGTTAG	
major - F	forward	GACGACTTGAAAAATGACGAAATC	From (Lehnertz et al., 2003)
major - R	reverse	CATATTCCAGGTCCTTCAGTGTGC	
Hprt1-F	forward	GCTTGCTGGTGAAAAGGACCTCTCGAAG	primer bank 7305155a1
Hprt1-R	reverse	CCCTGAAGTACTCATTATAGTCAAGGGCAT	
Luciferase-F	forward	AGAGATACGCCCTGGTTCCT	(Bui et al., 2009)
Luciferase-R	reverse	ATAAATAACGCGCCCAACAC	